

Sharp bounds of constants in Poincaré type inequalities for polygonal domains

S. Matculevich and S. Repin

Department of Mathematical Information Technology, University of Jyväskylä
 FIN-40100 Jyväskylä, FINLAND
 e-mails: svetlana.v.matculevich@jyu.fi, sergey.repin@jyu.fi

St. Petersburg Dept. of V.A. Steklov Institute of Mathematics of RAS
 St. Petersburg, Russia

December 3, 2024

Abstract

The paper is concerned with sharp estimates of constants in Poincaré type inequalities for functions having zero mean value on the boundary of a Lipschitz domain or on a measurable part of it. These estimates are useful for various numerical methods, in particular, for a posteriori error estimation methods for partial differential equations (PDEs). Therefore, we are mainly focused on domains typical for numerical analysis (simplexes in 2d and 3d) and suggest easily computable relations that provide sharp bounds of the respective constants. Also, we investigate numerically the behavior of the constants in the classical Poincaré inequalities and compare these results with known analytical estimates. In the last section, the estimates are used in order to obtain new a posteriori estimates for an elliptic boundary value problem.

1 Introduction

Let $\Omega \in \mathbb{R}^d$ ($d \geq 2$) be an open bounded connected domain with Lipschitz boundary $\partial\Omega$. Then, there exists a constant $C_{q,\Omega}$, $q \in (0, +\infty)$ (which depends only on Ω , q , and d) such that

$$\|w\|_{L^q(\Omega)} \leq C_{q,\Omega} \|\nabla w\|_{L^q(\Omega)}, \quad \forall w \in \tilde{H}^1(\Omega). \quad (1)$$

Here, $\tilde{H}^1(\Omega) := \left\{ w \in H^1(\Omega) \mid \{w\}_\Omega = 0 \right\}$, where $\{w\}_\Omega = \frac{1}{|\Omega|} \int_\Omega w \, dx$ is the mean value of w , and $|\Omega|$ is the Lebesgue measure of Ω .

Poincaré type inequalities also hold for functions having zero mean traces on the boundary or on a measurable part of it. Let

$$\tilde{H}^1(\Omega, \Gamma) := \left\{ w \in H^1(\Omega) \mid \{w\}_\Gamma = 0 \right\}, \quad (2)$$

where Γ is a part of $\partial\Omega$ such that $\text{meas}_{d-1}\Gamma > 0$. In particular, Γ may coincide with the whole boundary. For any $w \in \tilde{H}^1(\Omega, \Gamma)$, we have the estimates

$$\|w\|_{L^q(\Omega)} \leq C_{q,\Gamma}^p \|\nabla w\|_{L^q(\Omega)}, \quad (3)$$

$$\|w\|_{L^q(\Gamma)} \leq C_{q,\Gamma}^t \|\nabla w\|_{L^q(\Omega)}. \quad (4)$$

Poincaré type inequalities are often used in analysis of nonconforming approximations (e.g., discontinuous Galerkin or mortar methods), domain decomposition methods and other applications related to quantitative analysis of PDEs (see [6, 7, 13]). Therefore, values of constants (or sharp guaranteed upper bounds of them) are interesting from both analytical and computational points of view. They can be used in analysis of PDES considered on complicated domains and with nontrivial right-hand side. In order to provide sharp error estimate and consequently reliable and efficient computations, one requires the knowledge of the sharp bounds of constants described above.

It is known that for convex domains $C_{2,\Omega} \leq \frac{\text{diam}(\Omega)}{\pi}$, and $C_{1,\Omega} \leq \frac{\text{diam}(\Omega)}{2}$ (see [11] and [1], respectively). We assume (for simplicity) that $q = 2$ in all further discussions, therefore we neglect it. Improved upper estimates of C_Ω for isosceles triangles has been derived in [4]. They read as follows:

$$C_\Omega \leq \text{diam} T \cdot \begin{cases} \frac{1}{j_{1,1}} & \alpha \in (0, \frac{\pi}{3}], \\ \min \left\{ \frac{1}{j_{1,1}}, \frac{1}{j_{0,1}} (2(\pi - \alpha) \tan(\alpha/2))^{-1/2} \right\} & \alpha \in (\frac{\pi}{3}, \frac{\pi}{2}], \\ \frac{1}{j_{0,1}} (2(\pi - \alpha) \tan(\alpha/2))^{-1/2} & \alpha \in (\frac{\pi}{2}, \pi], \end{cases} \quad (5)$$

where $j_{0,1} \approx 2.4048$ and $j_{1,1} \approx 3.8317$ are the first positive roots of the Bessel functions J_0 and J_1 , respectively. The lower bound of C_Ω for convex domains (complimenting the Payne–Weinberger estimate) was derived in [3], where it was shown that

$$\frac{\text{diam } \Omega}{2j_{0,1}} \leq C_\Omega. \quad (6)$$

According to [2], this estimate is known to be the best lower bound among all known so far.

Exact values of C_Γ^p and C_Γ^t were derived in [9] for right triangles and rectangles. Below, we recall known constants for the certain simplexes, which are used further as the references in the estimates of the constants.

1. If $d = 2$, $T := \text{conv}\{(0,0), (0,h), (h,0)\}$, and $\Gamma := \{x_1 = 0, x_2 \in [0,h]\}$ coincides with one of the legs, then

$$C_\Gamma^p = \frac{h}{\zeta_0}, \quad \text{and} \quad C_\Gamma^t = \left(\frac{h}{\zeta_0 \tanh(\zeta_0)} \right)^{1/2}, \quad (7)$$

where ζ_0 and $\hat{\zeta}_0$ are the unique roots of the equations $z \cot(z) + 1 = 0$ and $\tan(z) + \tanh(z) = 0$ in $(0, \pi)$, respectively.

2. If $d = 2$, $T := \text{conv}\{(0,0), (0,h), (\frac{h}{2}, \frac{h}{2})\}$, and Γ coincides with the hypotenuse of the isosceles right triangle, then the constants are

$$C_\Gamma^p = \frac{h}{2\zeta_0}, \quad \text{and} \quad C_\Gamma^t = \left(\frac{h}{2} \right)^{1/2}, \quad (8)$$

with ζ_0 defined above in 1.

In numerical methods based on finite elements, we need the guaranteed estimates of the constants for a triangle in \mathbb{R}^2 as well as tetrahedrons in \mathbb{R}^3 . Therefore, the goal of the our paper is to obtain the sharp upper bounds of the constants in Poincaré type inequalities for the arbitrary non-generated simplexes and compare the theoretical estimates with lower bounds of the constants generated by numerical simulations.

In Section 2, we obtain guaranteed estimates of C_Γ^p and C_Γ^t for non-degenerate triangle by means of (3)–(4) on the reference triangles (studied in [9]) and the standard affine transformation of the coordinates in the multiple integral in \mathbb{R}^2 . In Section 3, we test the efficiency of the obtained theoretical upper bounds by comparing them to the lower bounds of the constants obtained by numerical simulations. Moreover, in the same section we compare the results of the numerical simulations of constants in classical Poincaré inequality on arbitrary triangles with upper and lower estimates studied in [11, 4, 3]. Section 4 is dedicated to attempt of combining numerical and theoretical ideas in order to derive bounds of the constants in Poincaré type inequalities for tetrahedrons in \mathbb{R}^3 . At last in Section 5, we present an example of an elliptic boundary value problem, where the estimates are used in order to obtain new a posteriori estimates for the error between approximate and exact solution.

2 Upper bounds of C_Γ^p and C_Γ^t for simplexes in \mathbb{R}^2

The goal of this section is to obtain sharp bounds of the constants in (3) and (4). For this purpose, we consider two basic triangles

$$\widehat{T}_I = \text{conv}\{(0,0), (1,0), (0,1)\} \quad \text{and} \quad \widehat{T}_{II} = \text{conv}\{(0,0), (1,0), (\frac{1}{2}, \frac{1}{2})\}, \quad (9)$$

with boundary

$$\widehat{\Gamma} = \{x_1 \in [0,1], x_2 = 0\}. \quad (10)$$

The efficient bounds of C_Γ^p and C_Γ^t follow from the Lemma below.

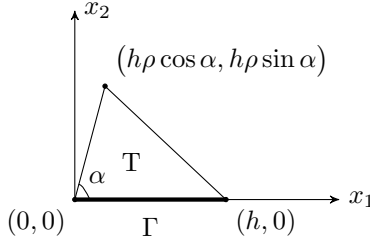


Figure 1: Arbitrary simplex T in \mathbb{R}^2 .

Lemma 1 For any $w \in \tilde{H}^1(T, \Gamma)$ defined on simplex

$$T = \text{conv} \left\{ (0,0), (h,0), (h\rho \cos \alpha, h\rho \sin \alpha) \right\}$$

with facet

$$\Gamma := \{x_1 \in [0, h]; x_2 = 0\},$$

the Poincaré type inequalities

$$\|w\|_T \leq \bar{C}_\Gamma^P h \|\nabla w\|_T \quad \text{and} \quad \|w\|_\Gamma \leq \bar{C}_\Gamma^t h^{1/2} \|\nabla w\|_T \quad (11)$$

hold with

$$\bar{C}_\Gamma^P = \min \left\{ \bar{c}_{p,I} C_{\hat{\Gamma},I}^P, \bar{c}_{p,II} C_{\hat{\Gamma},II}^P \right\} \quad \text{and} \quad \bar{C}_\Gamma^t = \min \left\{ \bar{c}_{\gamma,I} C_{\hat{\Gamma},I}^t, \bar{c}_{\gamma,II} C_{\hat{\Gamma},II}^t \right\}, \quad (12)$$

respectively. Here, the weighting parameters

$$\bar{c}_{p,I} = \mu_I^{1/2}, \quad \bar{c}_{p,II} = \mu_{II}^{1/2}, \quad \bar{c}_{\gamma,I} = (\rho \sin \alpha)^{-1/2} \bar{c}_{p,I}, \quad \bar{c}_{\gamma,II} = (2\rho \sin \alpha)^{-1/2} \bar{c}_{p,II}, \quad (13)$$

$$\mu_I(\rho, \alpha) = \frac{1}{2} \left(1 + \rho^2 + (1 + \rho^4 + 2 \cos 2\alpha) \rho^2 \right)^{-1/2}, \quad (14)$$

$$\mu_{II}(\rho, \alpha) = 2\rho^2 - 2\rho \cos \alpha + 1 + ((2\rho^2 + 1)(2\rho^2 + 1 - 4\rho \cos \alpha + 4\rho^2 \cos 2\alpha))^{-1/2}, \quad (15)$$

and $C_{\hat{\Gamma},I}^P$, $C_{\hat{\Gamma},I}^t$ and $C_{\hat{\Gamma},II}^P$, $C_{\hat{\Gamma},II}^t$ are the constants in (3) and (4) for reference triangles \hat{T}_I and \hat{T}_{II} , respectively.

Proof. (i) Let $\mathcal{F}_I : \hat{T}_I \rightarrow T$ (see Fig. 1) be a linear mapping such that

$$x = \mathcal{F}_I(\hat{x}) = B_I \hat{x}, \quad \text{where} \quad B_I = \begin{pmatrix} h & \rho h \cos \alpha \\ 0 & \rho h \sin \alpha \end{pmatrix}, \quad \det B_I = \rho h^2 \sin \alpha. \quad (16)$$

We know that

$$\|\hat{w}\|_{\hat{T}_I} \leq C_{\hat{\Gamma},I}^P \|\nabla \hat{w}\|_{\hat{T}_I}, \quad \forall \hat{w} \in \tilde{H}^1(\hat{T}_I, \hat{\Gamma}), \quad (17)$$

where $C_{\hat{\Gamma},I}^P$ is known from (7). Note that

$$\|\hat{w}\|_{\hat{T}_I}^2 = \frac{1}{\rho h^2 \sin \alpha} \|w\|_T^2, \quad (18)$$

and

$$\begin{aligned} \|\nabla \hat{w}\|_{\hat{T}_I}^2 &= \frac{1}{\rho h^2 \sin \alpha} \int_T \left(h^2 \left(\frac{\partial w}{\partial x_1} \right)^2 + h^2 \rho^2 \left(\cos \alpha \frac{\partial w}{\partial x_1} + \sin \alpha \frac{\partial w}{\partial x_2} \right)^2 \right) dx \\ &\leq \frac{1}{\rho h^2 \sin \alpha} \int_T A \nabla w \cdot \nabla w dx, \end{aligned} \quad (19)$$

where

$$A = h^2 \begin{pmatrix} 1 + \rho^2 \cos^2 \alpha & \rho^2 \sin \alpha \cos \alpha \\ \rho^2 \sin \alpha \cos \alpha & \rho^2 \sin^2 \alpha \end{pmatrix}. \quad (20)$$

It is not difficult to see that

$$\lambda_{\max}(A) = \frac{1}{2}h^2\mu_I(\rho, \alpha), \quad \mu_I(\rho, \alpha) = \left(1 + \rho^2 + (1 + \rho^4 + 2\cos 2\alpha \rho^2)^{1/2}\right).$$

Hence, using (17), (18), and (19), we obtain

$$\|w\|_T \leq \bar{c}_{p,I} C_{\Gamma,I}^p h \|\nabla w\|_T, \quad \bar{c}_{p,I}(\rho, \alpha) = \mu_I^{1/2}(\rho, \alpha). \quad (21)$$

Next, consider (4) on \hat{T}_I

$$\|\hat{w}\|_{\hat{\Gamma}} \leq C_{\Gamma,I}^t \|\nabla \hat{w}\|_{\hat{T}_I}, \quad \forall \hat{w} \in \tilde{H}^1(\hat{T}_I, \hat{\Gamma}), \quad (22)$$

where $C_{\Gamma,I}^t$ is derived in (7). By using (22) and noting that

$$\|\hat{w}\|_{\hat{\Gamma}}^2 = \frac{1}{h} \|w\|_T^2,$$

we obtain

$$\|w\|_T \leq \bar{c}_{\gamma,I} C_{\Gamma,I}^t h^{1/2} \|\nabla w\|_T, \quad \bar{c}_{\gamma,I}(\rho, \alpha) = \left(\frac{\mu_I(\rho, \alpha)}{\rho \sin \alpha}\right)^{1/2}, \quad (23)$$

where $\mu_I(\rho, \alpha)$ is defined in (14).

(ii) Next, we consider another reference triangle \hat{T}_{II} and use the mapping

$$x = \mathcal{F}_{II}(\hat{x}) = B_{II} \hat{x}, \quad B_{II} = \begin{pmatrix} h & 2\rho h \cos \alpha - h \\ 0 & 2\rho h \sin \alpha \end{pmatrix}, \quad \det B_{II} = 2\rho h^2 \sin \alpha.$$

By similar arguments, we find that for any $w \in \tilde{H}^1(T, \Gamma)$

$$\|w\|_T \leq \bar{c}_{p,II} C_{\Gamma,II}^p h \|\nabla w\|_T, \quad \bar{c}_{p,II}(\rho, \alpha) = \mu_{II}^{1/2}(\rho, \alpha), \quad (24)$$

and

$$\|w\|_T \leq \bar{c}_{\gamma,II} C_{\Gamma,II}^t h^{1/2} \|\nabla w\|_T, \quad \bar{c}_{\gamma,II}(\rho, \alpha) = \left(\frac{\mu_{II}(\rho, \alpha)}{2\rho \sin \alpha}\right)^{1/2}, \quad (25)$$

where $\mu_{II}(\rho, \alpha)$ is defined in (15).

(iii) Now, (11) follows from (21), (23), (24), and (25).

3 Lower bounds of C_{Γ}^p and C_{Γ}^t for simplexes in \mathbb{R}^2

Guaranteed upper bounds of the constants in (3) and (4) are provided by Lemma 1. Lower bounds can be found by minimization of the Rayleigh quotients

$$\mathcal{R}_{\Gamma}^p[u] = \min_{w \in \tilde{H}^1(T)} \frac{\|\nabla w\|_T}{\|w - \{w\}_{\Gamma}\|_T} \quad \text{and} \quad \mathcal{R}_{\Gamma}^t[u] = \min_{w \in \tilde{H}^1(T)} \frac{\|\nabla w\|_T}{\|w - \{w\}_{\Gamma}\|_{\Gamma}}, \quad (26)$$

if $\tilde{H}^1(T)$ is replaced by a finite dimensional subspace formed with the help of suitable anzats of trial functions. For this purpose, we use either power or Fourier series, i.e.,

$$\Phi^N := \text{span} \left\{ x^i y^j \right\}, \quad \Psi^N := \text{span} \left\{ \cos(\pi i x) \cos(\pi j y) \right\}, \quad i, j = 0, \dots, N, \quad i = j \neq 0, \quad (27)$$

where $\dim \Phi^N = \dim \Psi^N = M = (N+1)^2 - 1$. The corresponding constants obtained from the numerical simulations are denoted by $\underline{C}_{\Gamma}^{M,p}$ and $\underline{C}_{\Gamma}^{M,t}$, where M indicates the amount of basis functions. Spaces Φ^N and Ψ^N are also used

for analysis of $\mathcal{R}_T[u] = \min_{w \in \tilde{H}^1(T)} \frac{\|\nabla w\|_T}{\|w - \{w\}_T\|_T}$, which corresponds to the constant in (1). Latter quotient is also investigated further in the current section, the corresponding lower bound of the constant is denoted by \underline{C}_T^M .

In Figs. 4a and 4c, we depict the lower bound $\underline{C}_T^{M,p}$ for $M = 48$ of constant in (3) (thin line) for arbitrary T with $\rho = \frac{\sqrt{2}}{2}$, $\rho = 1$, and with respect to $\alpha \in (0, \pi)$, and guaranteed estimates $\bar{C}_I^p = \bar{c}_{p,I} C_{\hat{T},I}^p$ and $\bar{C}_{II}^p = \bar{c}_{p,II} C_{\hat{T},II}^p$ (dashed lines). The bold line corresponds to the upper bound \bar{C}_T^p of Poncaré type constant defined in (11). Since the last one is computed as the minimum between two reference constants \bar{C}_I^p and \bar{C}_{II}^p , we obtain sharper upper bound than if we would only use one reference case. Analogously in Figs. 5a and 5b, the lower bound $\underline{C}_T^{M,t}$ for $M = 48$ of constant in (4) (thin line) is illustrated together with upper bound \bar{C}_T^t , which is defined in (11) as the minimum of constants $\bar{C}_I^t = \bar{c}_{\gamma,I} C_{\hat{T},I}^t$ and $\bar{C}_{II}^t = \bar{c}_{\gamma,II} C_{\hat{T},II}^t$ (dashed lines). Figs. 4b and 4d illustrate the change of the simplex T with $\rho = 1$ and $\rho = \frac{\sqrt{2}}{2}$, respectively, depending on changes of angle α . The data depicted in Figs. 4a–5b is represented in Table 1 for convenience of the reader.

α	$\rho = \frac{\sqrt{2}}{2}$				$\rho = 1$			
	$\underline{C}_T^{48,p}$	\bar{C}_T^p	$\underline{C}_T^{48,t}$	\bar{C}_T^t	$\underline{C}_T^{48,p}$	\bar{C}_T^p	$\underline{C}_T^{48,t}$	\bar{C}_T^t
$\pi/18$	0.2429	0.2657	1.2786	1.5386	0.3245	0.3486	1.2572	1.6971
$\pi/9$	0.2414	0.2627	0.9289	1.0838	0.3248	0.3493	0.9058	1.2116
$\pi/6$	0.2389	0.2577	0.7919	0.8792	0.3268	0.3527	0.7632	1.0118
$2\pi/9$	0.2379	0.2507	0.7259	0.7543	0.3339	0.3636	0.6906	0.9201
$5\pi/18$	0.2632	0.2722	0.6945	0.7503	0.3514	0.3884	0.6529	0.9003
$\pi/3$	0.3008	0.3220	0.6829	0.8348	0.3809	0.4269	0.6362	0.8634
$7\pi/18$	0.3382	0.3694	0.6840	0.8432	0.4173	0.4721	0.6332	0.7840
$4\pi/9$	0.3740	0.4140	0.6947	0.7973	0.4556	0.5187	0.6404	0.7162
$\pi/2$	0.4075	0.4554	0.7136	0.7801	0.4929	0.4929	0.6560	0.6560
$5\pi/9$	0.4382	0.4933	0.7409	0.7973	0.5280	0.5340	0.6797	0.7162
$11\pi/18$	0.4660	0.5165	0.7779	0.8432	0.5600	0.5710	0.7125	0.7840
$2\pi/3$	0.4905	0.5361	0.8274	0.9118	0.5884	0.6037	0.7569	0.8634
$13\pi/18$	0.5115	0.5552	0.8948	1.0040	0.6129	0.6318	0.8175	0.9607
$7\pi/9$	0.5289	0.5720	0.9898	1.1292	0.6332	0.6550	0.9033	1.0874
$5\pi/6$	0.5426	0.5856	1.1334	1.3107	0.6492	0.6733	1.0332	1.2673
$8\pi/9$	0.5524	0.5956	1.3796	1.6118	0.6607	0.6865	1.2565	1.5623
$17\pi/18$	0.5583	0.6017	1.9436	2.2851	0.6676	0.6944	1.7692	2.2179

Table 1: Lower and upper bounds of C_T^p and C_T^t with respect to α and for $\rho = \frac{\sqrt{2}}{2}$ and 1.

Let us consider the triangle T with $\rho = \frac{\sqrt{2}}{2}$ (see corresponding Fig. 4a). We can see that in the point corresponding to $\alpha = \frac{\pi}{4}$ the lower bound $\underline{C}_T^{M,p}$ coincides with constant C_T^p (\bar{C}_{II}^p), because at this angle the transformation of \hat{T}_{II} to T is identical (see, e.g., Fig. 4d). Same behavior can be observed for (C_T^t) \bar{C}_{II}^t in Fig. 5a. In Fig. 4c, curve corresponding to $\underline{C}_T^{M,p}$ coincides with the curve illustrating the bound C_T^p (\bar{C}_I^p) at the point $\alpha = \frac{\pi}{2}$ due to the fact that T coincides with the reference triangle \hat{T}_I (see Fig. 4b). Analogical behavior is illustrated Fig. 5b for $\underline{C}_T^{M,t}$ and C_T^t (\bar{C}_I^t). Observations above are summarized in the Table 2. We consider two arbitrary simplexes, where one coincides with the reference triangle \hat{T}_I ($\alpha = \frac{\pi}{2}$, $h = 1$, and $\rho = 1$), and another coincides with \hat{T}_{II} ($\alpha = \frac{\pi}{4}$, $h = 1$, and $\rho = \frac{\sqrt{2}}{2}$). For both cases, $\bar{c}_{p,I}$, $\bar{c}_{\gamma,I}$ and $\bar{c}_{p,II}$, $\bar{c}_{\gamma,II}$ in (12) must be equal to 1. This fact is confirmed by the Table 2, in which lower bounds of the weighting parameters converge to 1, if M increases.

N	M	$\alpha = \frac{\pi}{2}, \rho = 1$		$\alpha = \frac{\pi}{4}, \rho = \frac{\sqrt{2}}{2}$	
		$\underline{c}_{p,I}^M$	$\underline{c}_{\gamma,I}^M$	$\underline{c}_{p,II}^M$	$\underline{c}_{\gamma,II}^M$
1	3	0.8801	0.9561	0.8647	1.0000
2	8	0.9945	0.9898	0.9925	1.0000
3	15	0.9999	0.9998	0.9962	1.0000
4	24	1.0000	0.9999	1.0000	1.0000
5	35	1.0000	1.0000	1.0000	1.0000
6	48	1.0000	1.0000	1.0000	1.0000

Table 2: Convergence of weighting parameters $\underline{c}_{p,I}^M$, $\underline{c}_{\gamma,I}^M$ and $\underline{c}_{p,II}^M$, $\underline{c}_{\gamma,II}^M$ with respect to increasing N and M .

In addition to lower and upper bounds of constants in (3) and (4), we also study respective eigenfunctions. First, we compare approximate and exact eigenfunctions corresponding to the lower bounds $\underline{C}_\Gamma^{M,p}$, $\underline{C}_\Gamma^{M,t}$ and exact constants C_Γ^p , C_Γ^t , respectively, for $T \equiv \widehat{T}_I$. According to [9], the minimizer of Rayleigh quotient $\mathcal{R}_\Gamma^p[w]$ associated with eigenvalue $\lambda_\Gamma^p = \left(\frac{z_0}{h}\right)^2$ has the form

$$u_\Gamma^p = \cos\left(\frac{z_0 x_1}{h}\right) + \cos\left(\frac{z_0(x_2 - h)}{h}\right),$$

where z_0 is the root of the equation $z \cot(z) + 1 = 0$ on $(0, \pi)$. It is depicted in Fig. 7a. Similarly, the minimizer of Rayleigh quotient $\mathcal{R}_\Gamma^t[w]$ associated with the minimum eigenvalue $\lambda_\Gamma^t = \frac{\hat{z}_0 \tanh(\hat{z}_0)}{h}$ is the following:

$$u_\Gamma^t = \cos(\hat{z}_0 x_1) \cosh(\hat{z}_0(x_2 - h)) + \cosh(\hat{z}_0 x_1) \cos(\hat{z}_0(x_2 - h)).$$

Here, \hat{z}_0 is the root of the equation $\tan(x) + \tanh(x) = 0$ on $(0, \pi)$ (see Fig. 9a). The eigenfunctions $u_\Gamma^{M,p}$ and $u_\Gamma^{M,t}$ are illustrated in Fig. 7b and Fig. 9b, respectively.

Next, we consider eigenfunctions corresponding to the lower bounds of $\underline{C}_\Gamma^{M,p}$, $\underline{C}_\Gamma^{M,t}$ for arbitrary triangle T . In order to depict them in the unified form, we use barycentric coordinates $\lambda_i \in (0, 1)$, $i = 1, 2, 3$, and $\sum_{i=1}^3 \lambda_i = 1$. Assume that $\rho = 1$. For selected α and corresponding to it coordinates of vertexes of T , i.e., $\mathbf{r}_i = (x_i, y_i)$, $i = 1, 2, 3$, we have the following relation between barycentric and Cartesian coordinates:

$$\begin{pmatrix} x \\ y \end{pmatrix} = \begin{pmatrix} x_1 & x_2 & x_3 \\ y_1 & y_2 & y_3 \end{pmatrix} (\lambda_1, \lambda_2, \lambda_3)^T,$$

and

$$\begin{pmatrix} \lambda_1 \\ \lambda_2 \end{pmatrix} = \mathbf{B}^{-1}(\mathbf{r} - \mathbf{r}_3).$$

Here, $\mathbf{r} = (x, y)$ is the arbitrary point on T . In order to make eigenfunctions corresponding to different T comparable, we normalize them by the L^2 -norm of the corresponding gradient. The eigenfunctions on T with $\alpha < \frac{\pi}{6}$ and $\alpha > \frac{5\pi}{6}$ have practically the same shape and behavior as the one for $\alpha = \frac{\pi}{6}$ and $\frac{5\pi}{6}$, respectively, therefore we omit exposing them. Fig. 6 illustrates the change of the behavior of eigenfunctions corresponding to $\underline{C}_\Gamma^{M,p}$ and $\underline{C}_\Gamma^{M,t}$ on isosceles T with $\alpha = \frac{\pi}{4}$, $\frac{\pi}{2}$, $\frac{3\pi}{4}$, and $\frac{5\pi}{6}$.

We use the above discussed algorithm for numerical evaluation of the constant in (1) on arbitrary triangles T . The lower bound \underline{C}_T^M of the latter constant is approximated by $\mathcal{R}[u] = \min_{w \in \tilde{H}^1(T)} \frac{\|w - \{w\}_T\|_T}{\|\nabla w\|_T}$ by using the basis defined in (27). The obtained values are compared with upper and lower bounds derived in [11] and [3], respectively, i.e.,

$$\frac{\text{diam } T}{2j_{0,1}} =: \underline{C}_T \leq C_T \leq \overline{C}_T := \frac{\text{diam } T}{\pi}. \quad (28)$$

Due to [4], we know the improved upper bound for isosceles triangles T defined in (5), i.e.,

$$C_T \leq \overline{C}_T^{LS} := \text{diam } T \cdot \begin{cases} \frac{1}{j_{1,1}} & \alpha \in (0, \frac{\pi}{3}], \\ \min\left\{\frac{1}{j_{1,1}}, \frac{1}{j_{0,1}}(2(\pi - \alpha) \tan(\alpha/2))^{-1/2}\right\} & \alpha \in (\frac{\pi}{3}, \frac{\pi}{2}], \\ \frac{1}{j_{0,1}}(2(\pi - \alpha) \tan(\alpha/2))^{-1/2} & \alpha \in (\frac{\pi}{2}, \pi]. \end{cases} \quad (29)$$

First, we depict the above discussed \underline{C}_T^M for $M = 48$ together with its upper and lower estimates defined in (28) for T with $\rho = \frac{\sqrt{2}}{2}$, 1, and $\frac{3}{2}$. According to Figs. 13a–13c, \underline{C}_T^{48} indeed lies within admissible two-sided bound. Nevertheless, it is easy to see that the classical Payne–Weinberger upper bound overestimates the constant. Only the lower bound is asymptotically sharp for degenerate obtuse triangles, i.e., $\alpha \rightarrow \pi$. However in Fig. 14, it is easy to see that the improved upper bound \overline{C}_T^{LS} is more efficient for the asymptotic cases $\alpha \rightarrow 0$ and $\alpha \rightarrow \pi$. Moreover, the lower bound \underline{C}_T^{48} indeed converges to $\frac{\text{diam } T}{j_{1,1}}$ as T degenerate to interval for $\alpha \rightarrow 0$ (see [4]).

In Fig. 14, the change of the derivative of the dashed curve corresponding to \underline{C}_T^{48} in the point $\alpha = \frac{\pi}{3}$ can be explained by the fact that function, minimizing quotient $\mathcal{R}_T[w]$, changes. We consider three eigenfunctions $u_{T,1}^{48}$, $u_{T,2}^{48}$, and $u_{T,3}^{48}$ corresponding to three sorted in increasing order eigenvalues $\lambda_{T,1}^{48}$, $\lambda_{T,2}^{48}$, and $\lambda_{T,3}^{48}$, which we get from approximating $\mathcal{R}_T[w]$ on isosceles triangles. Fig. 8 illustrates these three eigenfunctions for T with angles $\alpha = \frac{\pi}{3}$,

$\frac{\pi}{3} + \varepsilon$, and $\frac{\pi}{3} - \varepsilon$. We can see that the function corresponding to the minimal eigenvalue switches, if $\alpha \geq \frac{\pi}{3}$ (see Figs. 8d–8i). The approximations $u_{T,1}^{48}$ and $u_{T,2}^{48}$ for equilateral T can be compared with the exact eigenfunctions

$$u_1 = \cos\left(\frac{2\pi}{3}(2x_1 - 1)\right) - \cos\left(\frac{2\pi}{\sqrt{3}}x_2\right) \cos\left(\frac{\pi}{3}(2x_1 - 1)\right) \quad \text{and} \quad (30)$$

$$u_2 = \sin\left(\frac{2\pi}{3}(2x_1 - 1)\right) + \cos\left(\frac{2\pi}{\sqrt{3}}x_2\right) \sin\left(\frac{\pi}{3}(2x_1 - 1)\right) \quad (31)$$

obtained in [8] and presented in Fig. 11 in barycentric coordinates. It is easy to observe that approximation $u_{T,1}^{48}$ from Fig. 8d resembles with u_1 (see Fig. 11b), and $u_{T,2}^{48}$ from Fig. 8e identical to u_2 in Fig. 11a. The change of the minimizing function can be only seen for isosceles triangles, it does not appear on T with $\rho = \frac{\sqrt{2}}{2}$ and $\frac{3}{2}$ (see Figs. 10 and 12). The eigenvalues as well as the constants corresponding to the eigenfunctions presented in Figs. 8, 10 and 12 are summarized in the Table 3.

		$\frac{\pi}{3} - \varepsilon$		$\frac{\pi}{3}$		$\frac{\pi}{3} + \varepsilon$	
	$u_{T,i}^M$	$\underline{C}_{T,i}^{48}$	$\lambda_{T,i}^{48}$	$\underline{C}_{T,i}^{48}$	$\lambda_{T,i}^{48}$	$\underline{C}_{T,i}^{48}$	$\lambda_{T,i}^{48}$
$\rho = 1$	$u_{T,1}^{48}$	0.2419	17.0951	0.2387	17.5463	0.2537	15.5404
	$u_{T,2}^{48}$	0.2229	20.1216	0.2387	17.5463	0.2355	18.0309
	$u_{T,3}^{48}$	0.1353	54.6024	0.1378	52.6396	0.1422	49.4818
$\rho = \frac{\sqrt{2}}{2}$	$u_{T,1}^{48}$	0.23137	18.6804	0.23671	17.8471	0.24336	16.8850
	$u_{T,2}^{48}$	0.17082	34.2707	0.17435	32.8970	0.17642	32.1295
	$u_{T,3}^{48}$	0.1229	66.2058	0.12789	61.1402	0.13298	56.5493
$\rho = \frac{3}{2}$	$u_{T,1}^{48}$	0.34714	8.2983	0.35523	7.9247	0.3648	7.5143
	$u_{T,2}^{48}$	0.24485	16.6801	0.24885	16.1482	0.25125	15.8412
	$u_{T,3}^{48}$	0.18258	29.9981	0.19084	27.4575	0.19845	25.3921

Table 3: \underline{C}_T^M and λ_T^M corresponding to first three approximate eigenfunctions in Figs. 8, 10, and 12.

4 Estimates of C_Γ^p and C_Γ^t for tetrahedrons in \mathbb{R}^3

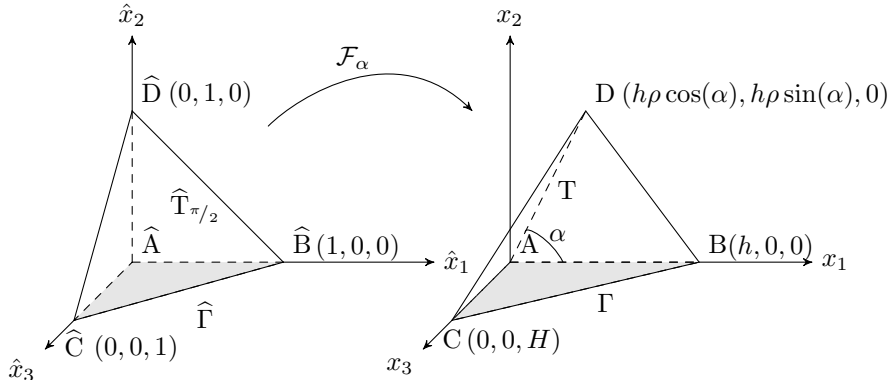


Figure 2: Mapping of tetrahedron $\hat{T}_{\pi/2}$ to $T \in \mathbb{R}^3$.

In the current section, we consider the arbitrary tetrahedron in \mathbb{R}^3 , i.e.,

$$T = \{(0,0,0), (h,0,0), (0,0,H), (D_{x_1}, D_{x_2}, D_{x_3})\} \quad (32)$$

with zero boundary

$$\Gamma = \{(0,0,0), (h,0,0), (0,0,H)\}. \quad (33)$$

We can restrict degrees of freedom of vertex D by either allowing it change the position only in the plane 0_{XY} with parameters $\alpha \in (0, \pi)$ and $\rho > 0$ (see Fig. 2), i.e., $(D_{x_1}, D_{x_2}, D_{x_3}) = (h\rho \cos \alpha, h\rho \sin \alpha, 0)$. Further, we also consider vertex D , which changes the azimuthal angle, i.e., $(D_{x_1}, D_{x_2}, D_{x_3}) = (h\rho \cos \alpha \sin \theta, h\rho \sin \alpha \sin \theta, h\rho \cos(\theta))$ (see Fig. 3).

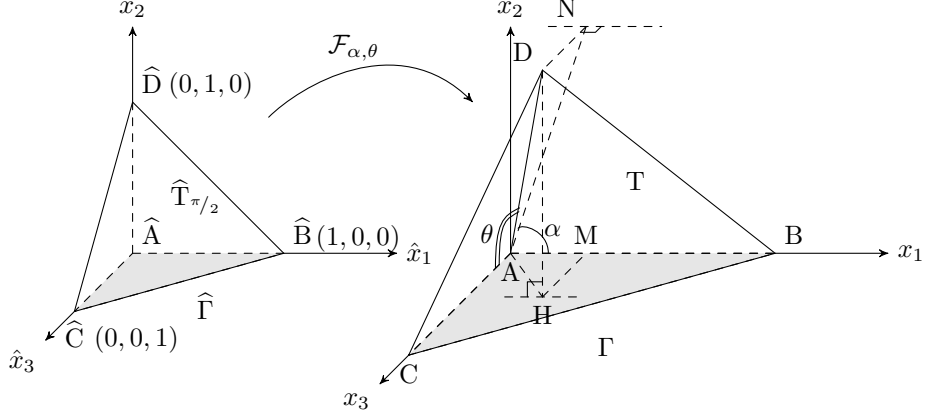


Figure 3: Mapping of tetrahedron $\widehat{T}_{\pi/2, \pi/2}$ to $T \in \mathbb{R}^3$.

Analogously to arbitrary triangles in \mathbb{R}^2 , we approximate constants C_{Γ}^p and C_{Γ}^t in Poincaré type inequalities by simulating $\mathcal{R}_{\Gamma}^p[w]$ and $\mathcal{R}_{\Gamma}^t[w]$. For this we consider function v from $H^1(T)$, where latter one is replaced by finite dimensional subspace formed with the help of suitable anzats of trial functions in \mathbb{R}^3 , i. e.,

$$\Phi^N := \left\{ \varphi_{ijk} = x^i y^j z^k, \quad i, j, k = 0, \dots, N, \quad i = j = k \neq 0 \right\}, \quad (34)$$

where $\dim \Phi^N = M = (N + 1)^3 - 1$.

Analogously to the method used in Lemma 1, the Poincaré type inequalities for the arbitrary tetrahedron T have the following form

$$\|v\|_T \leq C_{\Gamma}^p h H \|\nabla v\|_T, \quad C_{\Gamma}^p = \min_{r=1, \dots, R} \left\{ \bar{c}_{p,r} C_{\Gamma,r}^p \right\}, \quad (35)$$

$$\|v\|_{\Gamma} \leq C_{\Gamma}^t (hH)^{1/2} \|\nabla v\|_T, \quad C_{\Gamma}^t = \min_{r=1, \dots, R} \left\{ \bar{c}_{\gamma,r} C_{\Gamma,r}^t \right\}, \quad (36)$$

where $C_{\Gamma,r}^p$ and $C_{\Gamma,r}^t$ are the constants of r -th reference tetrahedron (out of R in total), and $\bar{c}_{p,r}$ and $\bar{c}_{\gamma,r}$ are auxiliary weighting parameters obtained from the transformation of each reference tetrahedron \widehat{T}_r to arbitrary T .

Since to authors knowledge there are no results on exact values of constants in Poincaré type inequalities for simplexes in \mathbb{R}^3 , we consider several reference tetrahedrons with $\rho = 1$, $\theta = \frac{\pi}{2}$, and $\alpha \in (0, \pi)$, for which the constants are calculated with high precision. In Table 4, we present the convergence of constants with respect to increasing M for angles $\alpha = \frac{\pi}{4}, \frac{\pi}{3}, \frac{\pi}{2}$, and $\frac{2\pi}{3}$.

Below, we illustrate the application of (36) in numerical simulations. Assume that we have only two reference tetrahedrons with $\alpha = \frac{\pi}{3}, \frac{\pi}{2}$ and $\theta = \frac{\pi}{2}$, i.e., $\widehat{T}_{\pi/3}$ and $\widehat{T}_{\pi/2}$ (corresponding to them constants $C_{\Gamma, \pi/2}^p$, $C_{\Gamma, \pi/2}^t$, $C_{\Gamma, \pi/3}^p$, and $C_{\Gamma, \pi/3}^t$ are taken from Table 4) and vertex D changes its position only in 0_{XY} , i.e., $(D_{x_1}, D_{x_2}, D_{x_3}) = (h\rho \cos(\alpha), h\rho \sin(\alpha), 0)$. The weights

$$\bar{c}_{p, \pi/2} = \max \left\{ \mu_{\pi/2}^{1/2} / H, 1/h \right\}, \quad \bar{c}_{\gamma, \pi/2} = (\rho \sin(\alpha))^{-1/2} \bar{c}_{p, \pi/2}, \quad (37)$$

and

$$\bar{c}_{p, \pi/3} = \max \left\{ \mu_{\pi/3}^{1/2} / H, 1/h \right\}, \quad \bar{c}_{\gamma, \pi/3} = \left(\rho \frac{2}{\sqrt{3}} \sin(\alpha) \right)^{-1/2} \bar{c}_{p, \pi/3}, \quad (38)$$

	$\alpha = \frac{\pi}{4}$	$\alpha = \frac{\pi}{3}$	$\alpha = \frac{\pi}{2}$	$\alpha = \frac{2\pi}{3}$				
M	$\underline{C}_{\Gamma}^{M,p}$	$\underline{C}_{\Gamma}^{M,t}$	$\underline{C}_{\Gamma}^{M,p}$	$\underline{C}_{\Gamma}^{M,t}$	$\underline{C}_{\Gamma}^{M,p}$	$\underline{C}_{\Gamma}^{M,t}$	$\underline{C}_{\Gamma}^{M,p}$	$\underline{C}_{\Gamma}^{M,t}$
7	0.32430	0.76010	0.32599	0.65465	0.36053	0.6547	0.41521	0.68616
26	0.33854	0.82945	0.34027	0.76128	0.37367	0.7516	0.42748	0.86332
63	0.34112	0.83133	0.34256	0.76290	0.37559	0.7520	0.42864	0.86460
124	0.34115	0.83134	0.34259	0.76291	0.37560	0.7520	0.42867	0.86463
215	0.34115	0.83134	0.34259	0.76291	0.37560	0.75200	0.42867	0.86463

Table 4: Convergence of the constants with respect to increasing M for T with $\rho = 1$, $\theta = \frac{\pi}{2}$, and several α .

with

$$\mu_{\pi/2} = \frac{1}{2} \left(1 + \rho^2 + \left(1 + \rho^4 + 2\rho^2 \cos(2\alpha) \right)^{1/2} \right), \quad (39)$$

$$\mu_{\pi/3} = \frac{1}{2} \left(1 + \rho^2 - \rho \cos(\alpha) \right) + 2 \left(\frac{1}{9} \left(1 + \rho^2 - \rho \cos(\alpha) \right)^2 - \frac{\rho^2}{3} \sin^2(\alpha) \right)^{1/2}, \quad (40)$$

are obtained by analyzing the following transformations

$$x = \mathcal{F}_{\pi/2}(\hat{x}) = B_{\pi/2} \hat{x}, \quad B_{\pi/2} = \begin{pmatrix} h & h\rho \cos(\alpha) & 0 \\ 0 & h\rho \sin(\alpha) & 0 \\ 0 & 0 & H \end{pmatrix},$$

$$x = \mathcal{F}_{\pi/3}(\hat{x}) = B_{\pi/3} \hat{x}, \quad B_{\pi/3} = \begin{pmatrix} h & \frac{h}{\sqrt{3}}(2\cos(\alpha)\rho-1) & 0 \\ 0 & \frac{2h}{\sqrt{3}}\rho \sin(\alpha) & 0 \\ 0 & 0 & H \end{pmatrix},$$

of reference tetrahedrons $\widehat{T}_{\pi/2}$ and $\widehat{T}_{\pi/3}$, respectively, to arbitrary T .

In numerical tests for T with $H = 0.5, 1$ and $\rho = 1, \frac{\sqrt{2}}{2}$, we obtain estimates of $\underline{C}_{\Gamma}^{M,p}$ and $\underline{C}_{\Gamma}^{M,t}$ illustrated in Figs. 15 and 16, respectively. One can see that only for the case $H = 1$ and $\rho = 1$, the thin line, corresponding to the lower bound of the constants, coincides with the estimate (bold line).

Assume now that we have two more reference tetrahedrons $\widehat{T}_{\pi/4}$ and $\widehat{T}_{2\pi/3}$. Then, the corresponding weights

$$\bar{c}_{p,\pi/4} = \max \left\{ \mu_{\pi/2}^{1/2}/H, 1/h \right\}, \quad \bar{c}_{\gamma,\pi/4} = \left(\rho \frac{2}{\sqrt{3}} \sin(\alpha) \right)^{-1/2} \bar{c}_{p,\pi/4}, \quad (41)$$

and

$$\bar{c}_{p,2\pi/3} = \max \left\{ \mu_{\pi/3}^{1/2}/H, 1/h \right\}, \quad \bar{c}_{\gamma,2\pi/3} = \left(\rho \frac{2}{\sqrt{3}} \sin(\alpha) \right)^{-1/2} \bar{c}_{p,2\pi/3}, \quad (42)$$

where

$$\mu_{\pi/4} = 1 + \rho^2 - \sqrt{2} + \rho \cos(\alpha) \left((1 + \rho^2 - \sqrt{2}\rho^2 \cos(\alpha))^2 - 2\rho^2 \sin^2(\alpha) \right)^{1/2}, \quad (43)$$

$$\mu_{2\pi/3} = \frac{1}{2} \left(1 + \rho^2 + \rho \cos(\alpha) \right) + 2 \left(\frac{1}{9} \left(1 + \rho^2 + \rho \cos(\alpha) \right)^2 - \frac{\rho^2}{3} \sin^2(\alpha) \right)^{1/2}, \quad (44)$$

are derived by analyzing transformations

$$x = \mathcal{F}_{\pi/4}(\hat{x}) = B_{\pi/4}, \quad B_{\pi/4} = \begin{pmatrix} h & \sqrt{2}h\rho \cos(\alpha) - 1 & 0 \\ 0 & \sqrt{2}h\rho \sin(\alpha) & 0 \\ 0 & 0 & H \end{pmatrix}, \quad (45)$$

and

$$x = \mathcal{F}_{2\pi/3}(\hat{x}) = B_{2\pi/3}, \quad B_{2\pi/3} = \begin{pmatrix} h & \frac{h}{\sqrt{3}}(2\cos(\alpha) + 1) & 0 \\ 0 & \frac{2h}{\sqrt{3}}\sin(\alpha) & 0 \\ 0 & 0 & H \end{pmatrix}, \quad (46)$$

respectively. Therefore, the obtained estimate is based on the minimum between four reference constants. In Fig. 17, we can observe that upper bound of the constant has improved (compare to Fig. 16).

In general, once we allow to vertex D to change its azimuth, i.e., $(D_{x_1}, D_{x_2}, D_{x_3}) = (h\rho\cos(\alpha)\sin(\theta), h\rho\sin(\alpha)\sin(\theta), h\rho\cos(\theta))$, the transformation of the right tetrahedron to the arbitrary one (see Figure 3) takes the following form:

$$x = \mathcal{F}_{\alpha,\theta}(\hat{x}) = B_{\alpha,\theta}, \quad B_{\alpha,\theta} = \begin{pmatrix} h & h\rho\cos(\alpha)\sin(\theta) & 0 \\ 0 & h\rho\sin(\alpha)\sin(\theta) & 0 \\ 0 & h\rho\cos(\theta) & H \end{pmatrix}. \quad (47)$$

In order to obtain auxiliary weights $\bar{c}_{p,r}$ and $\bar{c}_{p,r}$ for current transformation, we solve the eigenvalue problem for operator

$$A = h^2 \begin{pmatrix} 1 + \rho^2 \cos^2(\alpha) \sin^2(\theta) & \frac{1}{2}\rho^2 \sin(2\alpha) \sin(\theta) & \frac{1}{2}\rho^2 \cos(\alpha) \sin(2\theta) \\ \frac{1}{2}\rho^2 \sin(2\alpha) \sin^2(\theta) & \rho^2 \sin^2(\alpha) \cos^2(\beta) & \frac{1}{2}\rho^2 \sin(\alpha) \sin(2\theta) \\ \frac{1}{2}\rho^2 \cos(\alpha) \sin(2\theta) & \frac{1}{2}\rho^2 \sin(\alpha) \sin(2\theta) & \frac{H^2}{h^2} + \rho^2 \cos^2(\theta) \end{pmatrix}. \quad (48)$$

The maximal eigenvalue of (48) is defined as follows

$$\mu_{\alpha,\theta} = F^{\frac{1}{3}} + \frac{A}{3h^2} + \frac{C}{9h^4 F^{\frac{1}{3}}}, \quad (49)$$

where

$$\begin{aligned} A &= H^2 + h^2(1 + \rho^2), \\ E &= H^2 \rho^2 \sin^2 \alpha \sin^2 \theta, \\ C &= H^4 + h^2 \left(h^2 - H^2 + h^2 \rho^2 (\rho^2 - 1) \right) + 2H^2 h^2 \rho^2 - 3 \sin^2 \theta h^2 \rho^2 \left(h^2 \sin^2 \alpha - H^2 + h^2 \right), \\ D &= 4 \left(H^2 + h^2 \rho^2 + \rho^2 \sin^2 \theta (H^2 - h^2) + h^2 \rho^2 \sin^2 \alpha \sin^2 \theta \right), \\ B &= 9 \left((1 + rho^2) h^6 \rho^2 \sin(\theta)^2 (\sin(\alpha)^2 - 1) + H^4 h^2 \rho^2 \sin(\theta)^2 (H^2 + h^2 rho^2) \right) - 18 h^4 E \\ &\quad + 3 \left(H^2 h^2 (h^2 + H^2) + h^6 \rho^2 (1 + \rho^2) \right) - 2 \left(h^6 (1 + \rho^6) + H^6 \right) + 6 \left(H^2 h^2 \rho^2 (h^2(1 - \rho^2) - H^2) \right), \\ F &= \left(\frac{B^2}{2916 h^{12}} - \frac{C^3}{729 h^{12}} \right)^{\frac{1}{2}} + \frac{A^3}{27 h^6} - \frac{4AD}{96 h^4} + \frac{E}{2 h^2}. \end{aligned}$$

The numerical results with the lower bound of the constants as well as the upper bound are presented with respect to the angle $\alpha \in (0, \pi)$ and $\theta \in (0, \pi)$ in Figs. 18 and 19. Figs. 18a and 19a are view on estimates from the azimuth and elevation angles $(-45^\circ, 30^\circ)$, and Figs. 18b and 19b are from $(-135^\circ, 30^\circ)$. As expected, the bounds of $\underline{C}_{\Gamma}^{M,p}$ and $\underline{C}_{\Gamma}^{M,t}$ for the tetrahedron with $\alpha = \frac{\pi}{2}$ and $\theta = \frac{\pi}{2}$ are sharp, since the mapping $\mathcal{F}_{\pi/2, \pi/2}$ is identical. For convenience of the reader, the values of the lower and upper bounds of constants C_{Γ}^p and C_{Γ}^t from Figs. 18 and 19 are presented in Tables 5 and 6, respectively. As in the example above, one can construct the bounds based on two and more reference tetrahedrons, which would improve the estimates.

5 A posteriori estimates of approximation errors

In order to show possible application of the sharp upper bounds of above studied constants, we consider the example with the domain of complicated geometry and nontrivial boundary conditions (typically studied in numerical

		$\alpha = \frac{\pi}{6}$		$\alpha = \frac{\pi}{4}$		$\alpha = \frac{\pi}{3}$		$\alpha = \frac{\pi}{2}$	
θ	$\underline{C}_{\Gamma}^{M,p}$	\overline{C}_{Γ}^p	$\underline{C}_{\Gamma}^{M,p}$	\overline{C}_{Γ}^p	$\underline{C}_{\Gamma}^{M,p}$	\overline{C}_{Γ}^p	$\underline{C}_{\Gamma}^{M,p}$	\overline{C}_{Γ}^p	
$\pi/6$	0.23883	0.52694	0.24621	0.52253	0.25870	0.51792	0.29484	0.51308	
$\pi/4$	0.23883	0.52253	0.24621	0.51308	0.25870	0.50261	0.29484	0.49075	
$\pi/3$	0.29666	0.51792	0.31194	0.50261	0.33489	0.48413	0.38976	0.46002	
$\pi/2$	0.34302	0.51308	0.34112	0.49075	0.34256	0.46002	0.37559	0.37560	
$2\pi/3$	0.40428	0.51792	0.40562	0.50261	0.40927	0.48413	0.42867	0.46002	
$3\pi/4$	0.42890	0.52253	0.43110	0.51308	0.43505	0.50261	0.45017	0.49075	
$5\pi/6$	0.44964	0.52694	0.45193	0.52253	0.45539	0.51792	0.46607	0.51308	
		$\alpha = \frac{\pi}{2}$		$\alpha = \frac{2\pi}{3}$		$\alpha = \frac{3\pi}{4}$		$\alpha = \frac{5\pi}{6}$	
θ	$\underline{C}_{\Gamma}^{M,p}$	\overline{C}_{Γ}^p	$\underline{C}_{\Gamma}^{M,p}$	\overline{C}_{Γ}^p	$\underline{C}_{\Gamma}^{M,p}$	\overline{C}_{Γ}^p	$\underline{C}_{\Gamma}^{M,p}$	\overline{C}_{Γ}^p	
$\pi/6$	0.29484	0.51308	0.33069	0.51792	0.34468	0.52253	0.35499	0.52694	
$\pi/4$	0.29484	0.49075	0.33069	0.50261	0.34468	0.51308	0.35499	0.52253	
$\pi/3$	0.38976	0.46002	0.43880	0.48413	0.45742	0.50261	0.47106	0.51792	
$\pi/2$	0.37559	0.37560	0.42865	0.46002	0.45017	0.49075	0.46607	0.51308	
$2\pi/3$	0.42867	0.46002	0.45997	0.48413	0.47457	0.50261	0.48598	0.51792	
$3\pi/4$	0.45017	0.49075	0.47204	0.50261	0.48239	0.51308	0.49064	0.52253	
$5\pi/6$	0.46607	0.51308	0.47972	0.51792	0.48607	0.52253	0.49115	0.52694	

Table 5: Lower bound $\underline{C}_{\Gamma}^{M,p}$ for $M = 124$ and exact bounds \overline{C}_{Γ}^p .

		$\alpha = \frac{\pi}{6}$		$\alpha = \frac{\pi}{4}$		$\alpha = \frac{\pi}{3}$		$\alpha = \frac{\pi}{2}$	
θ	$\underline{C}_{\Gamma}^{M,t}$	\overline{C}_{Γ}^t	$\underline{C}_{\Gamma}^{M,t}$	\overline{C}_{Γ}^t	$\underline{C}_{\Gamma}^{M,t}$	\overline{C}_{Γ}^t	$\underline{C}_{\Gamma}^{M,t}$	\overline{C}_{Γ}^t	
$\pi/6$	1.09760	2.11000	0.96245	1.75944	0.91255	1.57581	0.93123	1.45274	
$\pi/4$	1.09760	1.75944	0.96245	1.45274	0.91255	1.28590	0.93123	1.16843	
$\pi/3$	0.89122	1.57581	0.79146	1.28590	0.75950	1.11924	0.78904	0.98969	
$\pi/2$	0.98017	1.45274	0.83132	1.16843	0.76290	0.98969	0.75199	0.75200	
$2\pi/3$	1.17698	1.57581	0.99473	1.28590	0.90578	1.11924	0.86463	0.98969	
$3\pi/4$	1.35195	1.75944	1.14144	1.45274	1.03737	1.28590	0.98220	1.16843	
$5\pi/6$	1.65317	2.11000	1.39424	1.75944	1.26490	1.57581	1.19017	1.45274	
		$\alpha = \frac{\pi}{2}$		$\alpha = \frac{2\pi}{3}$		$\alpha = \frac{3\pi}{4}$		$\alpha = \frac{5\pi}{6}$	
θ	$\underline{C}_{\Gamma}^{M,t}$	\overline{C}_{Γ}^t	$\underline{C}_{\Gamma}^{M,t}$	\overline{C}_{Γ}^t	$\underline{C}_{\Gamma}^{M,t}$	\overline{C}_{Γ}^t	$\underline{C}_{\Gamma}^{M,t}$	\overline{C}_{Γ}^t	
$\pi/6$	0.93123	1.45274	1.07244	1.57581	1.21573	1.75944	1.47044	2.11000	
$\pi/4$	0.93123	1.16843	1.07244	1.28590	1.21573	1.45274	1.47044	1.75944	
$\pi/3$	0.78904	0.98969	0.91773	1.11924	1.04309	1.28590	1.26357	1.57581	
$\pi/2$	0.75199	0.75200	0.86459	0.98969	0.98220	1.16843	1.19017	1.45274	
$2\pi/3$	0.86463	0.98969	0.96174	1.11924	1.08134	1.28590	1.30191	1.57581	
$3\pi/4$	0.98220	1.16843	1.07921	1.28590	1.20686	1.45274	1.44721	1.75944	
$5\pi/6$	1.19017	1.45274	1.29582	1.57581	1.44268	1.75944	1.72383	2.11000	

Table 6: Lower bound $\underline{C}_{\Gamma}^{M,t}$ for $M = 124$ and exact bounds \overline{C}_{Γ}^t .

analysis). Consider the following problem: find u such that

$$-\operatorname{div} p + \varrho^2 u = f, \quad \text{in } \Omega, \quad (50)$$

$$p = A \nabla u, \quad \text{in } \Omega, \quad (51)$$

$$u = u_D, \quad \text{on } \Gamma_D, \quad (52)$$

$$A \nabla u \cdot \mathbf{n} = F \quad \text{on } \Gamma_N, \quad (53)$$

where $f \in L^2(\Omega)$, $F \in L^2(\Gamma_N)$, $u_D \in H^1(\Omega)$, \mathbf{n} is the unit normal to Γ_N directed outwards, and $\lambda_1 |\xi|^2 \leq A \xi \cdot \xi$, where λ_1 is a positive constant independent of ξ . The generalized solution of (50)–(53) exists and is unique in the set $V_0 + u_D$, where $V_0 := \{w \in H^1(\Omega) \mid w = 0 \text{ on } \Gamma_D\}$.

Assume that $v \in V_0 + u_D$ is an conforming approximation of solution u of (50)–(53), and $e = u - v$. The guaranteed functional error estimate for the energy norm

$$\|e\| := \|\nabla e\|_A^2 + \|\varrho e\|^2, \quad (54)$$

where $\|\nabla e\|_A^2 := \int_{\Omega} A \nabla e \cdot \nabla e \, dx$, can be obtain from

$$\int_{\Omega} A \nabla e \cdot \nabla w \, dx + \int_{\Omega} \varrho^2 e w \, dx = \int_{\Omega} (f w - \varrho^2 v w - A \nabla v \cdot \nabla w) \, dx + \int_{\Gamma_N} F w \, ds, \quad \forall w \in V_0, \quad (55)$$

by introducing suitable vector valued function $\mathbf{y} \in H(\Omega, \text{div})$. The thorough theoretical study and applications of the functional estimates can be found in [10, 12, 5]. However, using inequalities (4) and (3) and technique of decomposing Ω into finite set of non-overlapping sub-domains, we can obtain computable majorants of the error, which operate with \mathbf{y} from a space wider than $H(\Omega, \text{div})$. This freedom can be used for getting more efficient error bounds.

Assume that Ω is polygonal (polyhedral) domain decomposed into a collection of non-overlapping sub-domains with Lipschitz continuous boundary. We assume that

$$\overline{\Omega} := \bigcup_{\Omega_i \subset \mathcal{O}_{\Omega}} \overline{\Omega}_i, \quad \mathcal{O}_{\Omega} := \left\{ \Omega_i \subset \Omega \mid \Omega_{i'} \cap \Omega_{i''} = \emptyset, i' \neq i'', i = 1, \dots, N \right\}. \quad (56)$$

By Γ_{int} we denote the set of all interior edges (faces) $\Gamma_{ij} = \overline{\Omega}_i \cap \overline{\Omega}_j$, and Γ_N be decomposed into $\Gamma_{iN} = \partial\Omega_i \cap \Gamma_N$. Define the space of vector valued functions

$$\begin{aligned} \hat{H}(\Omega, \mathcal{O}_{\Omega}, \text{div}) := \left\{ \mathbf{y} \in L^2(\Omega, \mathbb{R}^d) \mid \mathbf{y} = \mathbf{y}_i \in H(\Omega_i, \text{div}), \quad \left\{ \text{div} \mathbf{y}_i + f - \varrho^2 v \right\}_{\Omega_i} = 0, \Omega_i \in \mathcal{O}_{\Omega}, \right. \\ \left. \int_{\Gamma_{ij}} (\mathbf{y}_i - \mathbf{y}_j) \cdot \mathbf{n}_{ij} \, ds = 0, \Gamma_{ij} \subset \Gamma_{\text{int}}, \right. \\ \left. \int_{\Gamma_{iN}} (\mathbf{y}_i \cdot \mathbf{n}_i - F) \, ds = 0, \forall i = 1, \dots, N \right\}. \end{aligned} \quad (57)$$

Space $\hat{H}(\Omega, \mathcal{O}_{\Omega}, \text{div})$ is wider then $H(\Omega, \text{div})$, since here the pointwise continuity of the normal flux is replaced by a integral continuity. Therefore, by means of (55), integral identity

$$\begin{aligned} \sum_{i=1}^N \int_{\Omega_i} (\mathbf{y} \cdot \nabla w + \text{div} \mathbf{y} w) \, dx &= \sum_{\Gamma_{ij} \subset \Gamma_{\text{int}}} \int_{\Gamma_{ij}} (\mathbf{y}_i - \mathbf{y}_j) \cdot \mathbf{n}_{ij} w \, ds \\ &\quad + \sum_{\Gamma_{iN} \subset \Gamma_N} \int_{\Gamma_{iN}} (\mathbf{y}_i \cdot \mathbf{n}_i - F) w \, ds, \quad \forall w \in V_0, \mathbf{y} \in \hat{H}(\Omega, \mathcal{O}_{\Omega}, \text{div}), \end{aligned}$$

substitution $w = e$ into (55), and Hölder inequality, we find that

$$\begin{aligned} \|e\|^2 &\leq \|\mathbf{y} - A \nabla v\|_{A^{-1}} \|\nabla e\|_A + \sum_{i=1}^N \|f + \text{div} \mathbf{y}_i - \varrho^2 v\|_{\Omega_i} \left\| e - \{e\}_{\Omega_i} \right\|_{\Omega_i} \\ &\quad + \sum_{\Gamma_{ij} \subset \Gamma_{\text{int}}} \gamma_{ij} \left\| e - \{e\}_{\Gamma_{ij}} \right\|_{\Gamma_{ij}} + \sum_{\Gamma_{iN} \subset \Gamma_N} \gamma_{iN} \left\| e - \{e\}_{\Gamma_{iN}} \right\|_{\Gamma_{iN}}, \end{aligned} \quad (58)$$

where

$$\gamma_{ij} := \|(\mathbf{y}_i - \mathbf{y}_j) \cdot \mathbf{n}_{ij}\|_{\Gamma_{ij}}, \quad \gamma_{iN} := \|\mathbf{y}_i \cdot \mathbf{n}_i - F\|_{\Gamma_{iN}}. \quad (59)$$

Then, the last two terms can be estimated by using (4)

$$\begin{aligned} \|e\|^2 &\leq \|\mathbf{y} - A \nabla v\|_{A^{-1}} \|\nabla e\|_A + \sum_{i=1}^N \|f + \text{div} \mathbf{y}_i - \varrho^2 v\|_{\Omega_i} \left\| e - \{e\}_{\Omega_i} \right\|_{\Omega_i} \\ &\quad + \sum_{\Gamma_{ij} \subset \Gamma_{\text{int}}} \gamma_{ij} C_{\Gamma_{ij}}^t \|\nabla e\|_{\Omega_i} + \sum_{\Gamma_{iN} \subset \Gamma_N} \gamma_{iN} C_{\Gamma_{iN}}^t \|\nabla e\|_{\Omega_i}. \end{aligned} \quad (60)$$

If for each $\Omega_i \subset \mathcal{O}_\Omega$

$$C_{i,\max}^t := \max_{\Gamma_{ij} \subset \Gamma_{\text{int}} \cup \Gamma_{iN} \subset \Gamma_N} \left\{ C_{\Gamma_{ij}}^t, C_{\Gamma_{iN}}^t \right\}, \quad (61)$$

and

$$\eta_i = \left(\sum_{\Gamma_{ij} \cap \Omega_i \neq \emptyset} \xi_{ij} \right)^{1/2}, \quad \text{where} \quad \xi_{ij} = \begin{cases} \frac{1}{2} \gamma_{ij}, & \Gamma_{ij} \in \Gamma_{\text{int}}, \\ \gamma_{iN}, & \Gamma_{ij} \in \Gamma_N. \end{cases} \quad (62)$$

Then, (60) can be represented as follows:

$$\|e\|^2 \leq \|\mathbf{y} - A\nabla v\|_{A^{-1}} \|\nabla e\|_A + \sum_{i=1}^N \|f + \operatorname{div} \mathbf{y}_i - \varrho^2 v\|_{\Omega_i} \left\| e - \{e\}_{\Omega_i} \right\|_{\Omega_i} + \sum_{i=1}^N \eta_i C_{i,\max}^t \|\nabla e\|_{\Omega_i}. \quad (63)$$

The last term in (63) can be estimated by

$$\Upsilon(\mathbf{y}, \mathcal{O}_\Omega) \|\nabla e\|_\Omega, \quad \text{where} \quad \Upsilon(\mathbf{y}, \mathcal{O}_\Omega) := \left(\sum_{i=1}^N \left(C_{i,\max}^t \right)^2 \eta_i^2 \right)^{1/2},$$

and the second from the end in (63) by using (1)

$$\Phi(\mathbf{y}, \mathcal{O}_\Omega) \|\nabla e\|_\Omega, \quad \text{where} \quad \Phi(\mathbf{y}, \mathcal{O}_\Omega) := \left(\sum_{i=1}^N C_{2,\Omega_i}^2 \|f + \operatorname{div} \mathbf{y}_i - \varrho^2 v\|_{\Omega_i}^2 \right)^{1/2}.$$

Therefore, we arrive at the estimate

$$\|e\| \leq \|\mathbf{y} - A\nabla v\|_{A^{-1}} + \frac{1}{\lambda_1} \left(\Upsilon(\mathbf{y}, \mathcal{O}_\Omega) + \Phi(\mathbf{y}, \mathcal{O}_\Omega) \right). \quad (64)$$

Here, the term $\Upsilon(\mathbf{y}, \mathcal{O}_\Omega)$ controls violations of conformity of \mathbf{y} in the normal direction. It is easy to see that $\Upsilon(\mathbf{y}, \mathcal{O}_\Omega) = 0$, if $\mathbf{y} \cdot \mathbf{n}$ on the Γ_{int} are continuous. Here, it can be viewed as a measure of ‘flux nonconformity’. Other terms have the same meaning as in known form of a posteriori error estimates, namely, $\|\mathbf{y} - A\nabla v\|_{A^{-1}}$ measures the violation in duality relation (51), and $\Phi(\mathbf{y}, \mathcal{O}_\Omega)$ provides the reliability of the estimate by measuring the error in equilibrium (balance) equation (50).

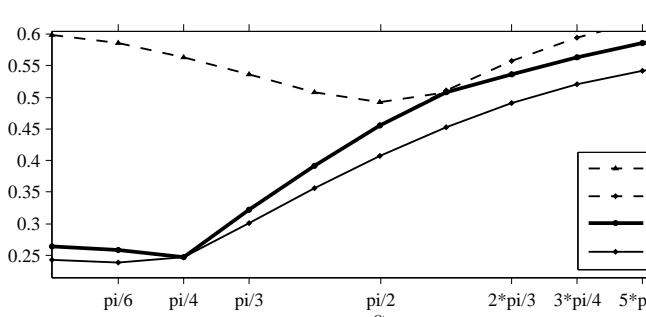
References

- [1] G. Acosta and R. G. Durán. An optimal Poincaré inequality in L^1 for convex domains. *Proc. Amer. Math. Soc.*, 132(1):195–202 (electronic), 2004.
- [2] R. Bañuelos and K. Burdzy. On the “hot spots” conjecture of J. Rauch. *J. Funct. Anal.*, 164(1):1–33, 1999.
- [3] S. Y. Cheng. Eigenvalue comparison theorems and its geometric applications. *Math. Z.*, 143(3):289–297, 1975.
- [4] R. S. Laugesen and B. A. Siudeja. Minimizing Neumann fundamental tones of triangles: an optimal Poincaré inequality. *J. Differential Equations*, 249(1):118–135, 2010.
- [5] O. Mali, P. Neittaanmäki, and S. Repin. *Accuracy verification methods*, volume 32 of *Computational Methods in Applied Sciences*. Springer, Dordrecht, 2014. Theory and algorithms.
- [6] S. Matculevich, P. Neittaanmäki, and S. Repin. A posteriori error estimates for time-dependent reaction-diffusion problems based on the Payne–Weinberger inequality. *AIMS*, 35(6), 2015.
- [7] S. Matculevich and S. Repin. Computable bounds of the distance to the exact solution of parabolic problems based on Poincaré type inequalities. *Zap. Nauchn. Sem. S.-Peterburg. Otdel. Mat. Inst. Steklov (POMI)*, 425(1):7–34, 2014.
- [8] B. J. McCartin. Eigenstructure of the equilateral triangle. II. The Neumann problem. *Math. Probl. Eng.*, 8(6):517–539, 2002.

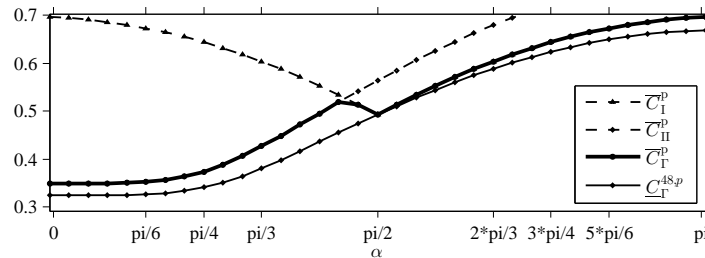
- [9] A. I. Nazarov and S. I. Repin. Exact constants in Poincaré type inequalities for functions with zero mean boundary traces. *Mathematical Methods in the Applied Sciences*, 2014. Published in arXiv.org in 2012, math/1211.2224.
- [10] P. Neittaanmäki and S. Repin. *Reliable methods for computer simulation*, volume 33 of *Studies in Mathematics and its Applications*. Elsevier Science B.V., Amsterdam, 2004. Error control and a posteriori estimates.
- [11] L. E. Payne and H. F. Weinberger. An optimal Poincaré inequality for convex domains. *Arch. Rational Mech. Anal.*, 5:286–292 (1960), 1960.
- [12] S. Repin. *A posteriori estimates for partial differential equations*, volume 4 of *Radon Series on Computational and Applied Mathematics*. Walter de Gruyter GmbH & Co. KG, Berlin, 2008.
- [13] S. Repin. Estimates of constants in boundary-mean trace inequalities and applications to error analysis. In *Numerical Mathematics and Advanced Applications - ENUMATH 2013*, volume 103 of *Lecture Notes in Computational Science and Engineering*, pages 215–223. Springer, Switzerland, 2015.

6 Appendix

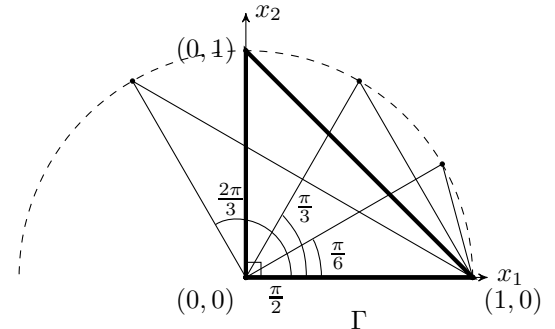
In this section, we collect all graphics cited in Section 3 and 4.



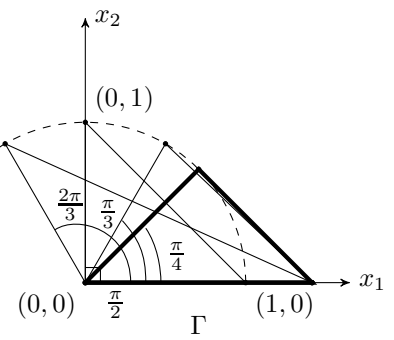
(a) $\rho = \frac{\sqrt{2}}{2}$



(c) $\rho = 1$

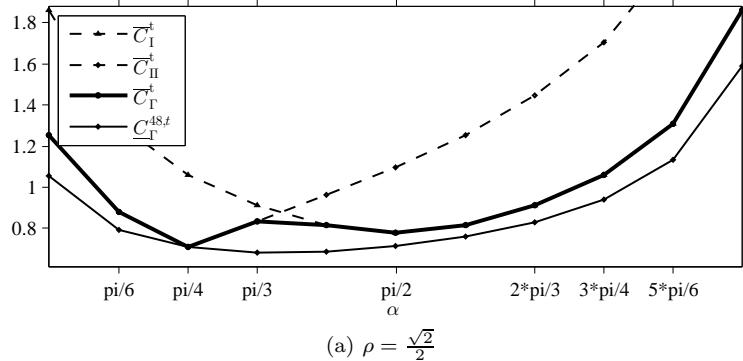


(b) $\rho = \frac{\sqrt{2}}{2}$

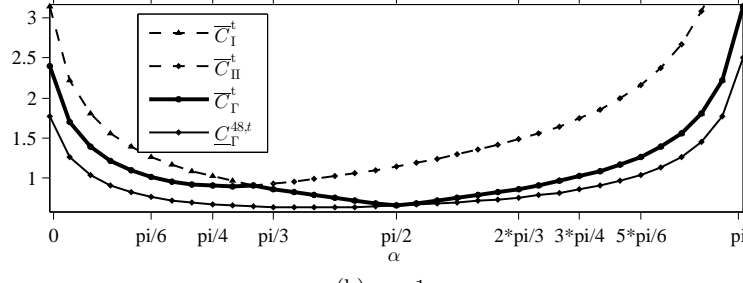


(d) $\rho = 1$

Figure 4: Lower and upper bounds of C_{Γ}^p for $\Gamma \in \mathbb{R}^2$ (a)-(b) $\rho = \frac{\sqrt{2}}{2}$ and (c)-(d) $\rho = 1$.



(a) $\rho = \frac{\sqrt{2}}{2}$



(b) $\rho = 1$

Figure 5: Lower and upper bound of C_{Γ}^t for $\Gamma \in \mathbb{R}^2$ (a) $\rho = \frac{\sqrt{2}}{2}$ and (b) $\rho = 1$.

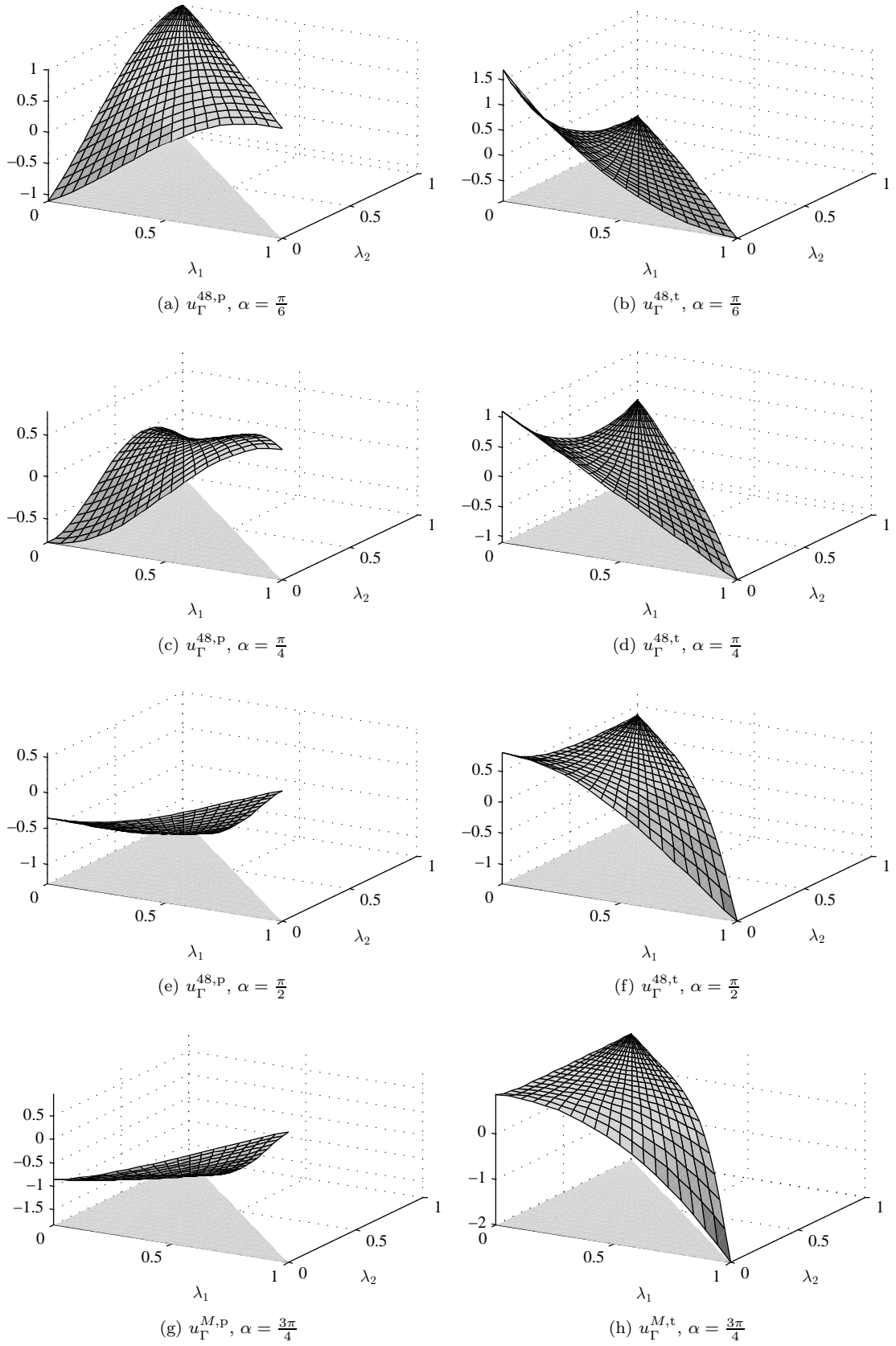


Figure 6: Eigenfunctions corresponding to $\underline{C}_{\Gamma}^{M,p}$ and $\underline{C}_{\Gamma}^{M,t}$ for $M = 48$ on simplexT with $\rho = 1$ and different α .

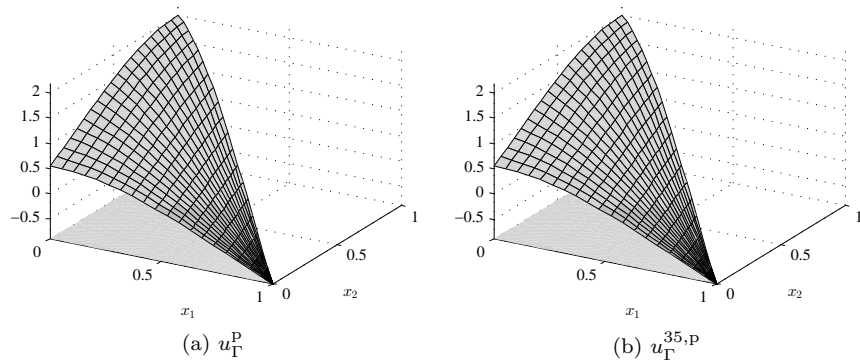


Figure 7: Exact and approximate eigenfunctions corresponding to C_{Γ}^p on $T \equiv \widehat{T}_I$.

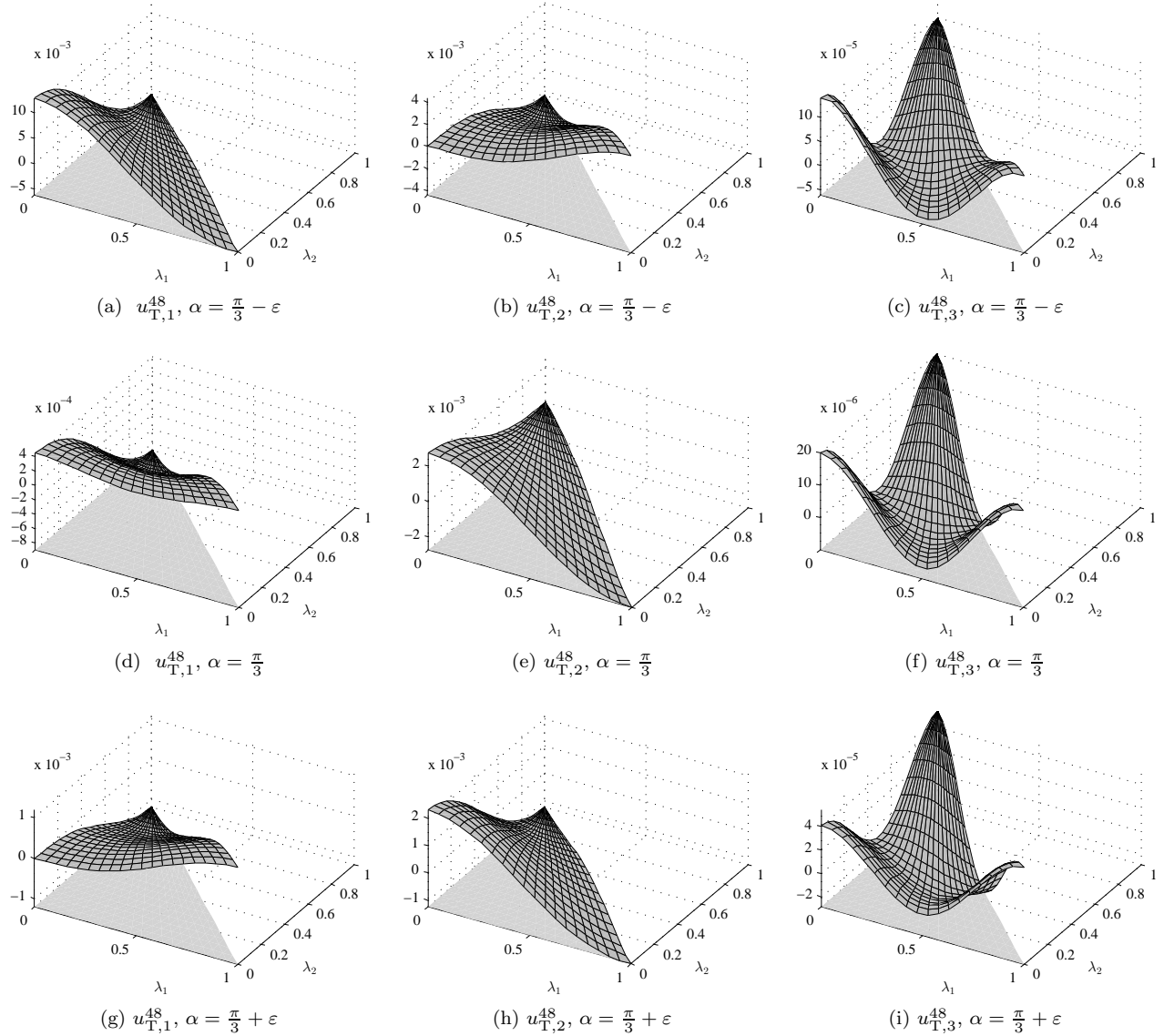


Figure 8: Eigenfunctions corresponding to \underline{C}_T^M with $M = 48$ on isosceles triangles $T \in \mathbb{R}^2$ with $\alpha = \frac{\pi}{3}$, $\frac{\pi}{3} - \varepsilon$, and $\frac{\pi}{3} + \varepsilon$ in barycentric coordinates.

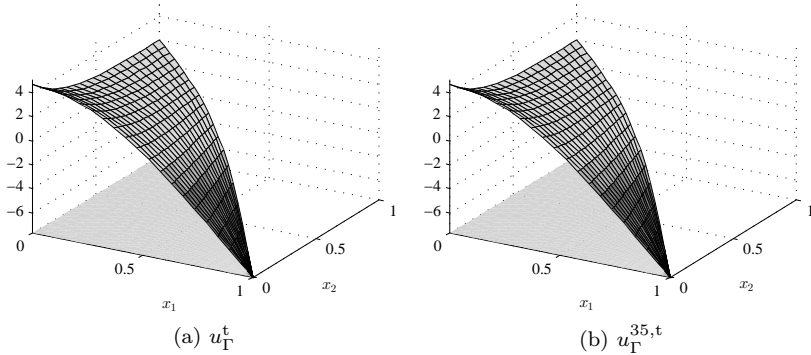


Figure 9: Exact and approximate eigenfunctions corresponding to \overline{C}_G^t on $T \equiv \widehat{T}_I$.

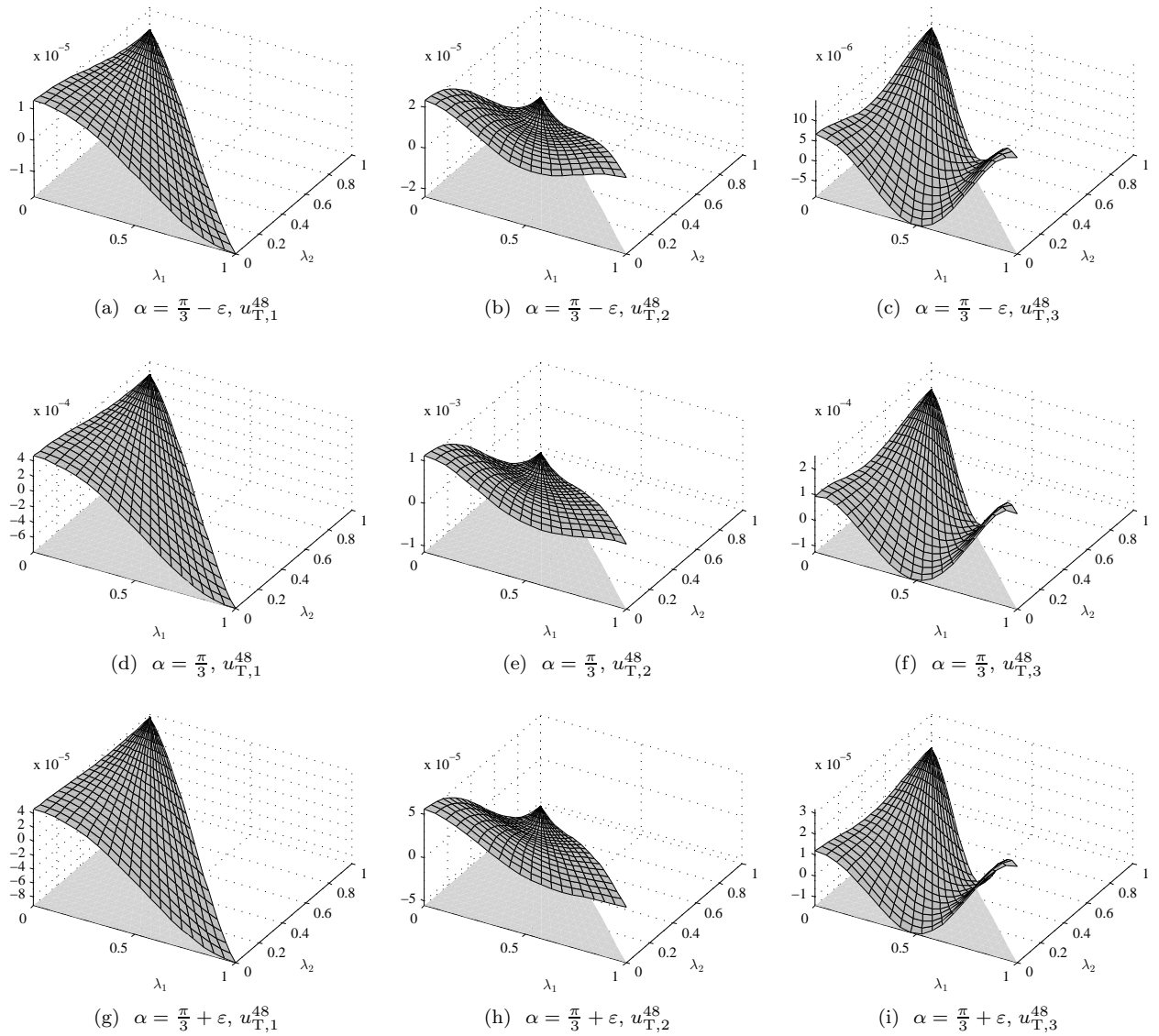


Figure 10: Eigenfunctions corresponding to \underline{C}_G^M for $M = 48$ on simplexes $T \in \mathbb{R}^2$ with $\rho = \frac{\sqrt{2}}{2}$, $\alpha = \frac{\pi}{3}$ and $\frac{\pi}{3} - \varepsilon$, $\frac{\pi}{3} + \varepsilon$ in barycentric coordinates.

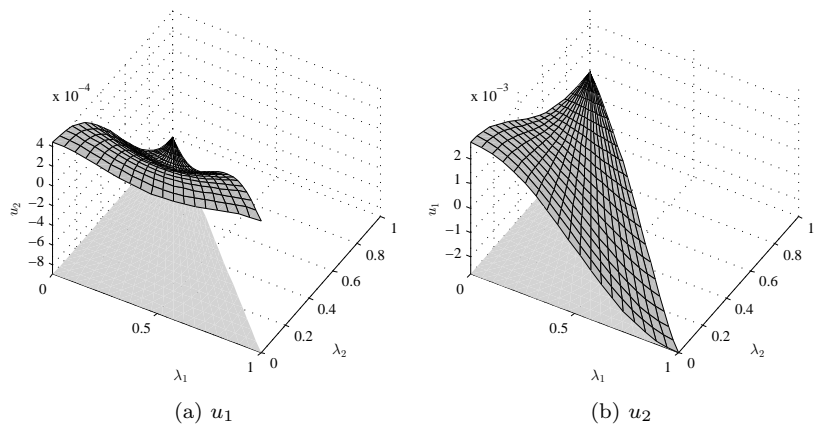


Figure 11: The first two exact eigenfunctions u_1 and u_2 of equilateral triangle in barycentric coordinates.

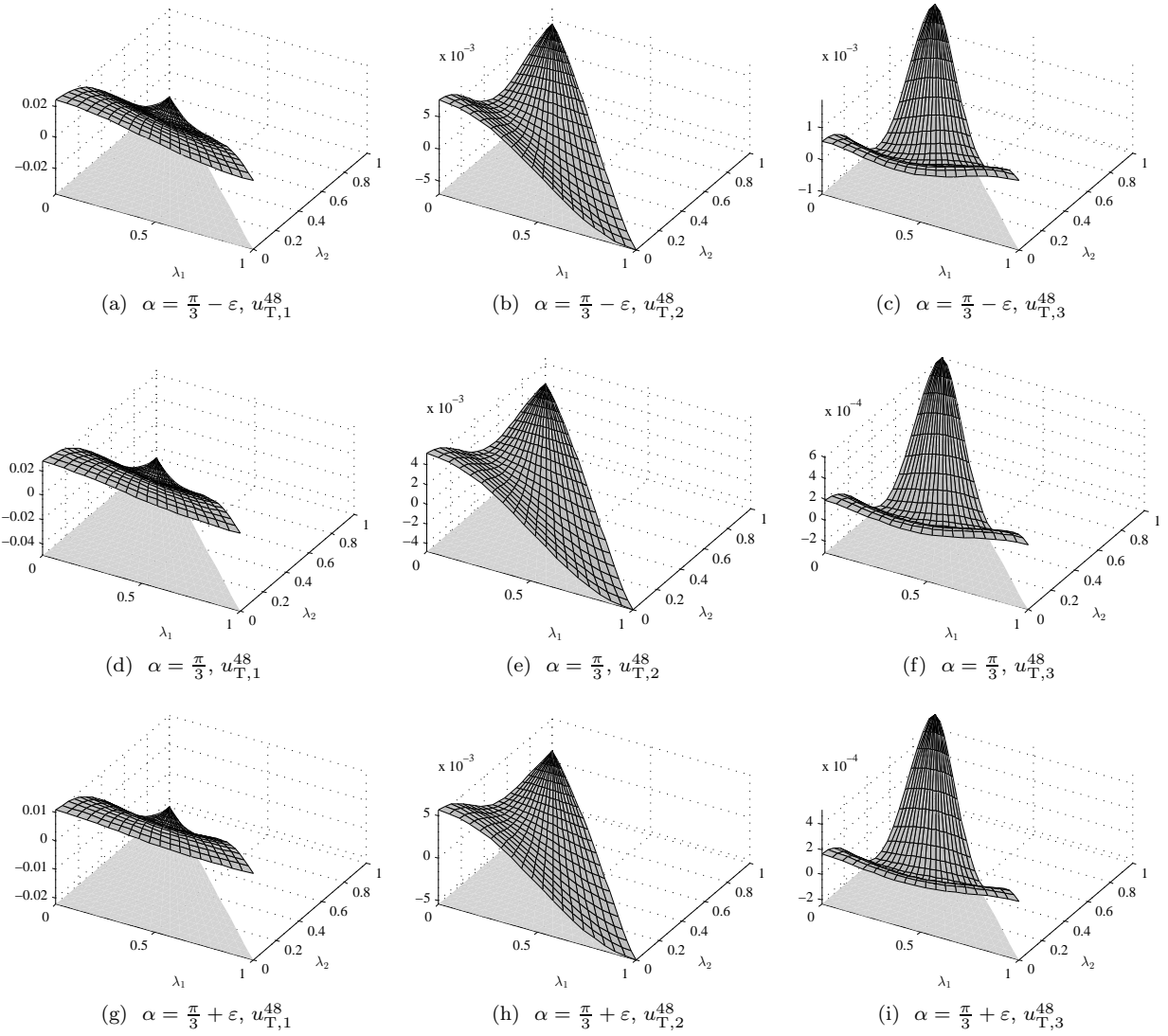


Figure 12: Eigenfunctions corresponding to \underline{C}_T^M for $M = 48$ on simplexes $T \in \mathbb{R}^2$ with $\rho = \frac{3}{2}$, $\alpha = \frac{\pi}{3}$ and $\frac{\pi}{3} - \varepsilon$, $\frac{\pi}{3} + \varepsilon$ in barycentric coordinates.

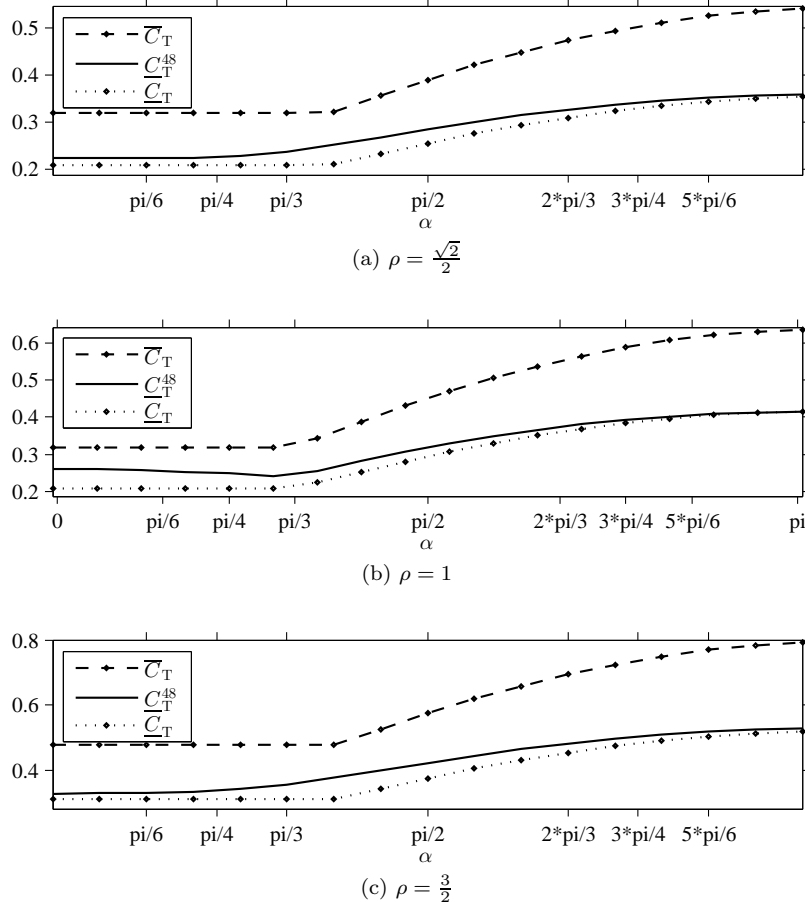


Figure 13: \underline{C}_T^{48} with upper and lower bounds with respect to α on T with (a) $\rho = \frac{\sqrt{2}}{2}$ and (b) $\frac{3}{2}$.

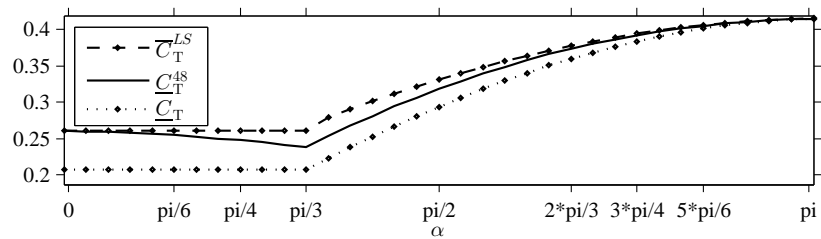


Figure 14: Approximation \underline{C}_T^{48} with improved upper and lower bounds on isosceles T with respect to α .

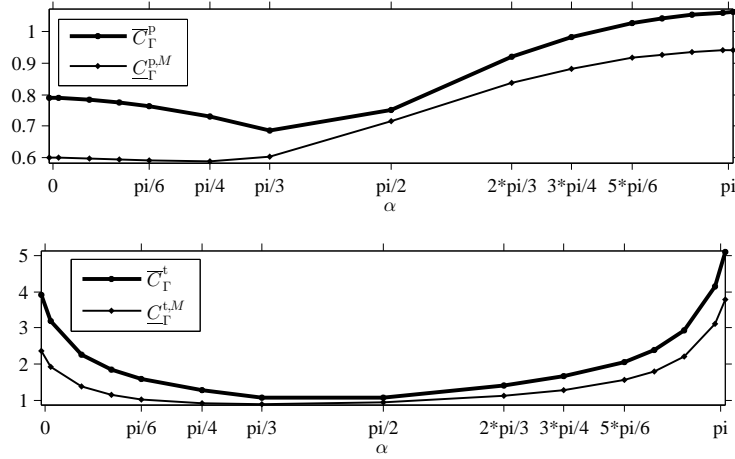


Figure 15: $\underline{C}_{\Gamma}^{M,p}$ and $\underline{C}_{\Gamma}^{M,t}$ for $T \in \mathbb{R}^3$ with $H = 0.5$, $\rho = 1$ and estimate based on two reference tetrahedrons.

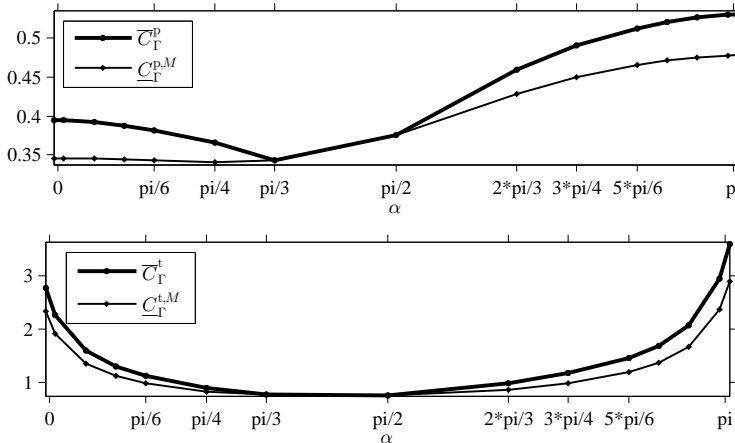


Figure 16: $\underline{C}_{\Gamma}^{M,p}$ and $\underline{C}_{\Gamma}^{M,t}$ for $T \in \mathbb{R}^3$ with $H = 1$, $\rho = 1$ and estimate based on two reference tetrahedrons..

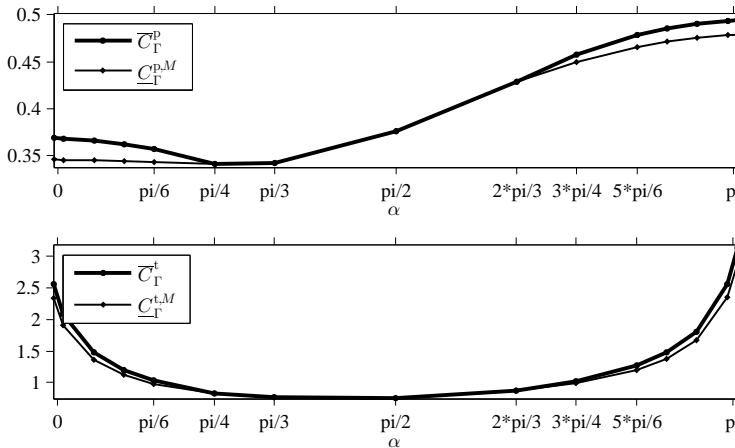


Figure 17: C_{Γ}^p and C_{Γ}^t for $T \in \mathbb{R}^3$ with $H = 1$, $\rho = 1$ with four reference tetrahedrons.

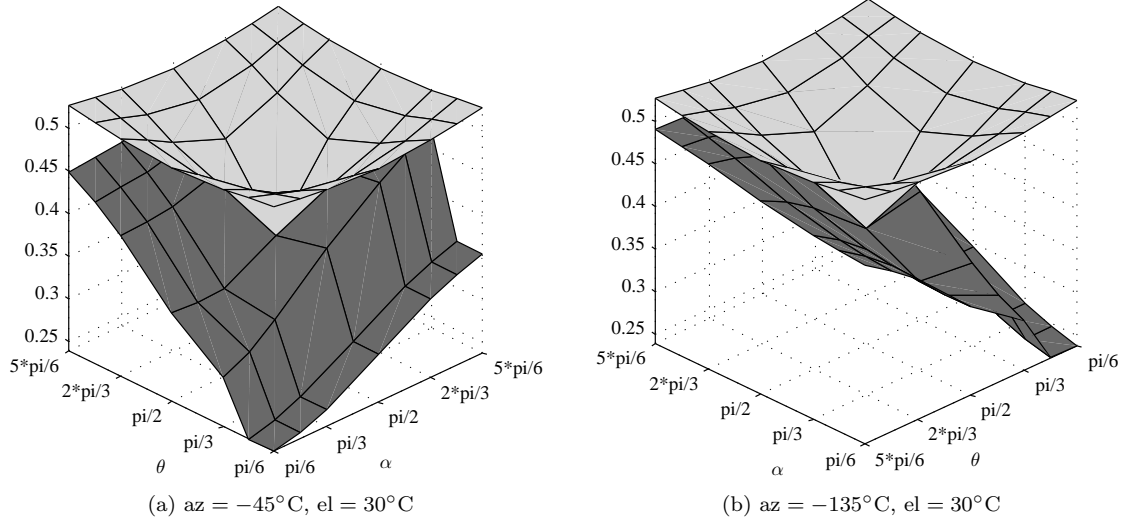


Figure 18: C_{Γ}^p with estimates based on transformation $\mathcal{F}_{\alpha,\theta}$.

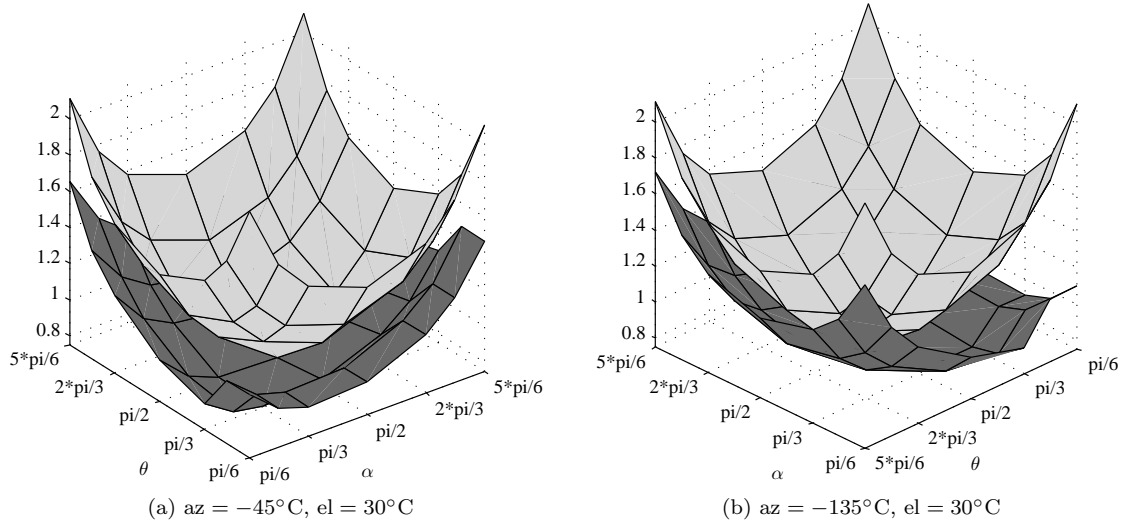


Figure 19: C_{Γ}^t with estimates based on transformation $\mathcal{F}_{\alpha,\theta}$.